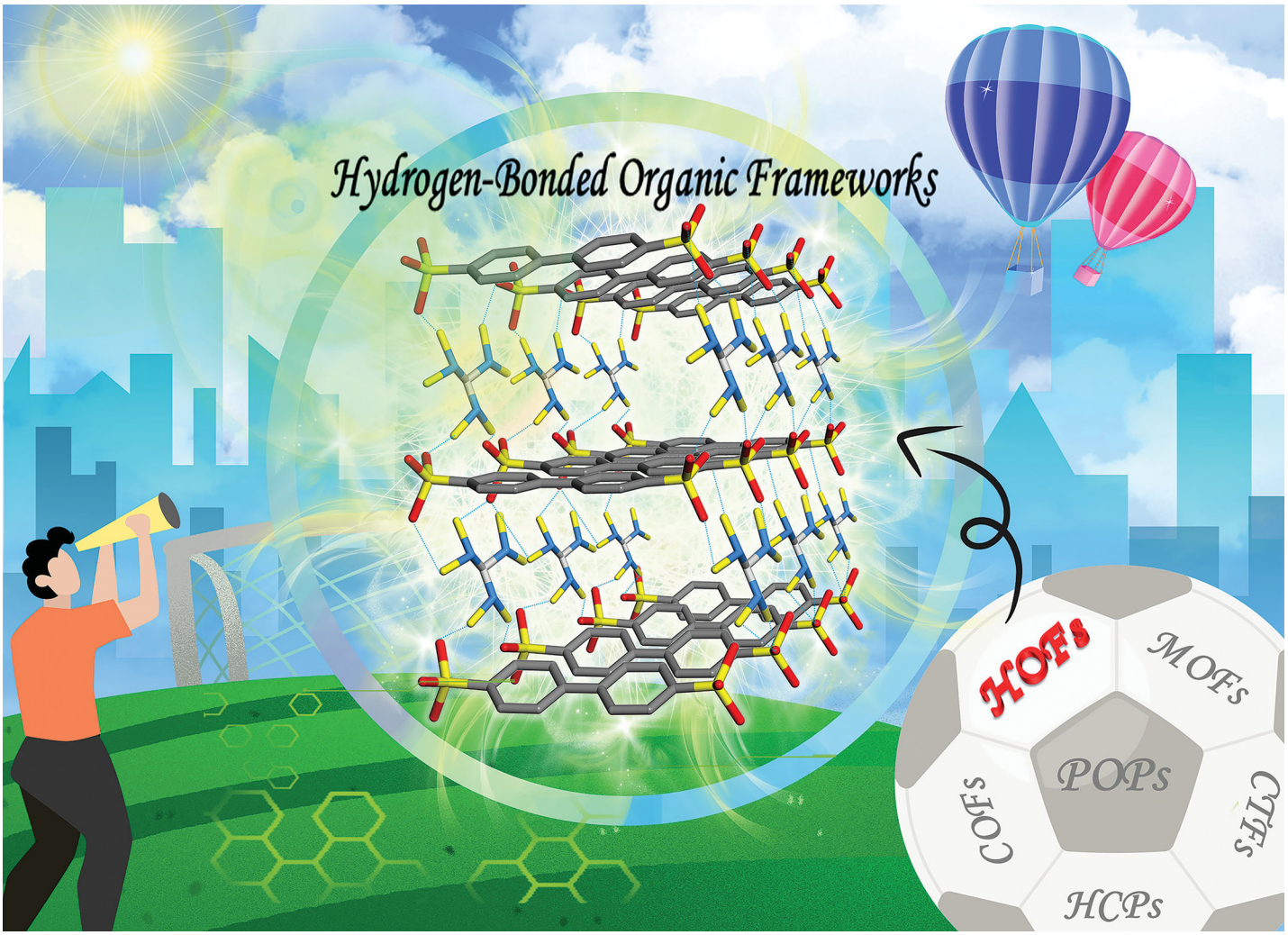

Showcasing research from Professor Shanlin Qiao's laboratory, College of Chemistry and Pharmaceutical Engineering, Hebei University of Science and Technology, Shijiazhuang, China.

Hydrogen-bonded organic frameworks: design, applications, and prospects

Hydrogen-bonded organic frameworks (HOFs) are a new type of porous crystalline material, which are assembled through intermolecular hydrogen bonds of organic building blocks. The unique advantages of HOFs, such as nonmetallic, self-repairing and easily deform abilities have attracted great research attention, enabling new platforms for exploring multifunctional applications in hydro-carbon separation, gas adsorption, proton conduction, sensing and fluorescence detection, catalysis, biomedicine.

As featured in:

See Haining Liu, Shanlin Qiao *et al.*, *Mater. Adv.*, 2022, **3**, 3680.

ROYAL SOCIETY OF CHEMISTRY

rsc.li/materials-advances

Registered charity number: 207890

Materials Advances

ROYAL SOCIETY OF CHEMISTRY

REVIEW

View Article Online
View Journal | View Issue

Cite this: *Mater. Adv.*, 2022, 3, 3680

Hydrogen-bonded organic frameworks: design, applications, and prospects

Lifang Chen,†[a] Boying Zhang,†[b] Liling Chen,[a] Haining Liu,*[a] Yongqi Hu[a] and Shanlin Qiao *[ac]

As a new type of porous crystalline material, hydrogen-bonded organic frameworks (HOFs) assemble through intermolecular hydrogen bonds of organic building blocks. The unique advantages of HOFs, such as high crystallinity, solution processability, and facile regeneration, have attracted great research attention, enabling new platforms for exploring multifunctional applications. Herein, we summarize basic principles and synthetic methods of constructing HOFs with favorable stability and permanent porosity. In addition, hydrogen bonding motifs (diaminotriazine (DAT), carboxylic acid (–COOH), sulfonic acid ($-SO_3H$), and others) used to construct HOFs and some potential applications of HOFs are highlighted, including gas separation and storage, proton conduction, sensing and fluorescence detection, ultra-long phosphorescent materials, light luminescent materials, catalysis, *etc.* Finally, the prospects and challenges of HOFs in the future are discussed.

Received 11th December 2021,
Accepted 20th February 2022

DOI: 10.1039/d1ma01173a

rsc.li/materials-advances

1. Introduction

Porous materials have been extensively explored in the past few years, and they have been widely utilized in many fields, such as sensing, catalysis, fluorescence detection, proton conduction, gas separation, storage, *etc.*[1–3] Porous materials include inorganic porous materials, inorganic–organic hybrid materials, and organic porous materials. As for the inorganic porous materials, mesoporous silica materials should not be missed. Mesoporous silica materials with an impressive ordered pore structure, tunable pore size distribution and diverse mesopore shapes have been widely used in adsorption and separation, industrial catalysis, biomedicine, environmental protection and other fields. However, there are still many problems, such as complicated synthesis, unclear structure and imprecise micro-control.

The development of the representative crystalline porous materials is illustrated in Fig. 1. Zeolite, a typical representative of crystalline inorganic materials, is a crystalline microporous aluminosilicate composed of corner-sharing SiO_4^- and AlO_4^- tetrahedra.[4] Zeolites are widely used in separation, adsorption, catalysis, and ion exchange due to their special chemical composition and unique porous structure.[5] Generally, zeolite-based materials are prepared through hydrothermal–solvothermal methods. However, a detailed molecular mechanism of zeolite nucleation is still ambiguous.[6,7] Moreover, zeolites exhibit poor structural diversity compared with other porous materials due to monomer restriction.

Metal–organic frameworks (MOFs), as a kind of inorganic–organic hybrid porous materials, have been widely investigated. MOFs are coordination polymers with a periodic network structure that is composed of inorganic metal centers (metal ions or metal clusters) and organic ligands,[8–12] featuring a flexible structure, abundant porosity, and tunable chemical composition. Nevertheless, the stability of MOFs (particularly in water) is still a critical issue, impeding their applications and further commercial development.[13,14] Moreover, various

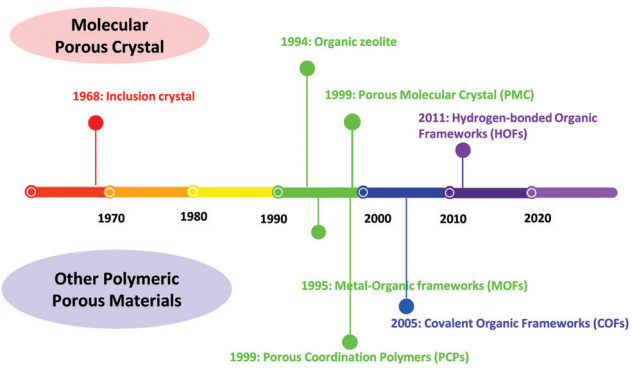

Fig. 1 Representative crystalline porous materials.

[a] College of Chemistry and Pharmaceutical Engineering, Hebei University of Science and Technology, Shijiazhuang 050018, China. E-mail: ccpeslqiao@hebust.edu.cn, liuhn@hebust.edu.cn
[b] Department of Chemical Engineering, Faculty of Engineering and the Built Environment, University of Johannesburg, Doornfontein 2028, South Africa
[c] Hebei Electronic Organic Chemicals Technology Innovation Center, Shijiazhuang 050018, China
† These authors contributed equally to this work.

coordination modes of organic ligands and metal atoms of MOFs give rise to structural diversity, but metal nodes in the framework may exhibit certain toxicity, limiting their applications.

Compared with MOFs, organic porous materials can effectively avoid the connection of metal nodes and have a lower skeleton density. Covalent organic frameworks (COFs) and porous molecular crystals (PMCs) are representative crystalline organic porous materials. It should be noted that COFs combine crystallinity, modular synthetic versatility, highly accessible surface area, and good physicochemical stability.[15–19] Due to these unique advantages, COFs have been applied in various fields, *e.g.*, gas separation and adsorption,[20–22] proton conduction[23,24] and catalysis.[25,26]

PMCs are assembled from discrete organic molecules *via* weak interactions.[27–29] Therefore, porous PMCs do not involve the formation of new and breaking of old chemical bonds during the preparation process. Molecules crystallize to form solvated crystals, which are further activated to remove the solvent, thereby creating pores.[30–33] However, the pore structure of some PMCs may collapse without support from solvent molecules. Historically, Chen[34] has renamed PMCs that form a framework with permanent pores through hydrogen bonding as hydrogen-bonded organic frameworks (HOFs) to distinguish them from PMCs with permanent pores.

HOFs represent a kind of novel crystalline porous polymers assembled from small organic molecules with light elements (C, H, O, N, B, and others) *via* weak hydrogen bonding, van der Waals forces, and π–π stacking interactions. Compared with other porous materials, HOFs exhibit unique features,[35,36] which can be summarized as follows: (i) *nonmetallic character:* HOFs are constructed using small organic molecules without metal elements through intermolecular hydrogen bonding. (ii) *High crystallinity:* hydrogen bond linkage in HOFs is weak, and a reversible process is induced during crystallization, yielding high crystallinity. (iii) *Self-repairing ability:* based on dynamic covalent chemistry, the formation of reversible bonds is controlled by thermodynamic equilibrium, allowing HOFs to self-repair under certain synthetic conditions. (iv) *Uncontrollability:* even though molecules are used as building blocks, ideal porous HOFs are not always obtained. (v) *Instability:* due to weak hydrogen bonding interaction, the pore structure of HOFs may easily deform. These characteristics make HOFs emerging functional materials facing both opportunities and challenges in further development and application.

However, there are few review articles summarizing HOF design strategies and synthesis methods in detail. In this review, design strategies and synthesis methods for constructing HOFs are summarized at first. Second, we summarize hydrogen bonding motifs that can be used to form HOFs. Furthermore, the major applications of HOFs in different fields are presented (Fig. 2), including hydrocarbon separation,[37–42] gas adsorption,[43–45] proton conduction,[46,47] sensing and fluorescence detection,[48–53] catalysis,[54–57] and biomedicine.[58] Finally, we also discuss the prospects and future developmental directions of HOFs.

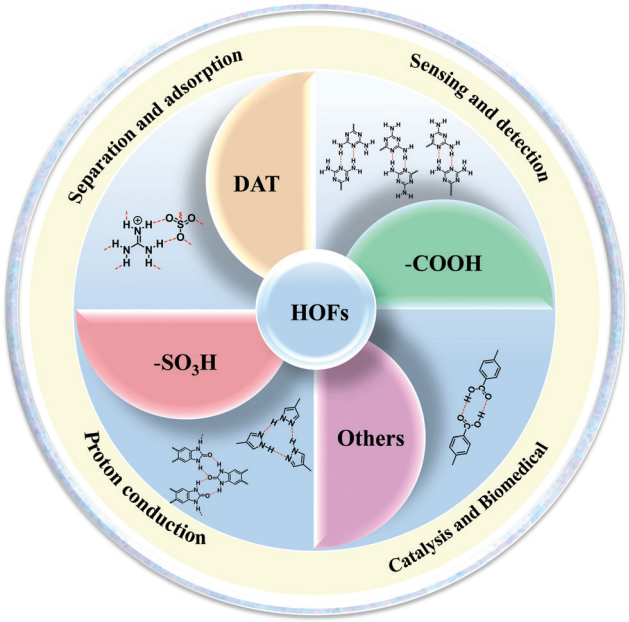

Fig. 2 Design and application of hydrogen-bonded organic framework materials.

2. Design principles and synthetic methods

In principle, an equal number of hydrogen bond donors and acceptors in an organic group is beneficial to forming HOFs, mainly because these hydrogen bond donors and acceptors can form inherent hydrogen bond units, like dimers,[59–61] trimers,[62] and even chain structures.[63,64] Moreover, the rigidity and directionality of a hydrogen bond building unit are stronger than those of a single hydrogen bond donor/acceptor pair. Therefore, an expanded framework with different pore and topological structures can be formed when a H-bond building unit is combined with an organic framework. Geometric shapes formed by the connection of hydrogen bond building units can be transmitted to the network. The pore size depends on the length of the organic framework.[34] Therefore, it is critical to choose suitable hydrogen bond building units for constructing HOFs with high porosity, but this is only the most basic principle to follow.

2.1 Design principles and strategies

HOFs are mainly connected through intermolecular hydrogen bonds. Hydrogen bonds have a certain directionality and a relatively strong non-covalent character. However, hydrogen bond interactions are very weak compared with covalent bonds and metal coordination bonds. A reversible process is induced during the crystallization of HOFs, yielding high crystallinity. At the same time, the stability of HOFs is relatively poor due to the reversibility of hydrogen bonds, limiting the possibility of synthesizing a multifunctional material. Therefore, it is still an arduous task to construct HOFs with high stability and permanent porosity, simultaneously overcoming weak hydrogen bond

interactions. Several strategies have been proposed in the following paragraphs to improve the rigidity and stability of HOFs.

2.1.1 Achieving stronger intermolecular interactions. The introduction of stronger intermolecular interactions is a direct strategy to improve the stability and rigidity of HOFs. There are two approaches to enhance intermolecular interactions for organic molecules toward their self-assembly into HOFs. The first approach is to build multiple hydrogen bonds. Due to the weak interaction of a single hydrogen bond, the HOF's stability may be significantly improved by creating multiple hydrogen bonds, *i.e.*, the more hydrogen bonds between organic ligand molecules, the more robust the entire framework.[13,29,34,65] Based on this approach of multiple hydrogen bonds between molecules, a HOF with a highly stable structure was constructed and denoted as HOF-2.[66] After HOF-2 was immersed in different alcohol solvents for 24 h, the 2θ values of the obtained XRD patterns remained unchanged. Even calcined HOF-2 maintained the original framework at a relatively high temperature (350 °C). The use of multiple hydrogen bonds provides a practical solution for the construction of highly stable HOFs. The second approach is to build charge-assisted hydrogen bonds between cations and anions. Foster has reported a highly stable HOF based on strong charge-assisted hydrogen bonds between amidine and carboxylate.[67] The HOF was exfoliated into nanosheets (HON) by ultrasonic treatment for 12 h in a strong polar DMF solvent and acetone. Each HON sample was heated at 80 °C for 3 days. X-ray diffraction showed that HONs maintained extended crystallinity. Furthermore, after water treatment, the AFM imaging revealed that the nanosheets maintained their monolayer properties. It is worth noting that highly stable HOFs were obtained only through charge-assisted hydrogen bonding.

To sum up, both of these above mentioned approaches for constructing stable HOFs have been experimentally verified. The multiple hydrogen bonds strategy is a good choice for obtaining satisfactory stability of the basic framework. Still, if there is a requirement for stability in water, charge-assisted hydrogen bonding is the best choice. Therefore, we should make a reasonable choice based on material requirements.

2.1.2 Selection of a rigid stereoscopic framework as a hydrogen bond building unit. Generally, a hydrogen bond building unit consists of a main chain and hydrogen bonding sites. The steric hindrance effect of rigid framework molecules may yield insufficient intermolecular accumulation, which is conducive to generating porous solids with permanent pores.[68,69] In 2021, Wang *et al.* reported a new diamondoid HOF denoted as ZJU-HOF-10.[70] ZJU-HOF-10 was constructed using a tetrahedral carboxylic building block. When the supercritical carbon dioxide (sc-CO_2) drying method was used to remove solvent molecules, the original framework did not collapse but porosity increased. The sc-CO_2-activated ZJU-HOF-10(sc) exhibited excellent separation performance for hydrocarbon separation (C_2H_4/C_2H_6). Therefore, although most porous organic solids connected by weak hydrogen bonding may be sensitive to desolvation, some rigid frameworks still exhibit permanent porosity. In summary, framework rigidity significantly affects the stability and permanent porosity of HOFs, so a rigid skeleton hydrogen bond unit is more beneficial to the HOF structure.

2.1.3 Introducing additional intermolecular interaction into HOFs. Although HOFs are mainly connected by hydrogen bonding, the participation of other weak interactions is also indispensable. The weak interaction between molecules such as π–π interaction is an important driving force for the construction of organic porous solids. 2D HOFs with strong thermal and chemical stability have been synthesized, termed as HOF-10x (x = 0, 1, 2),[71] from a pyrene group with systematically extended π-conjugated molecular arms. The decomposition temperatures of HOF-10x (x = 0, 1, 2) were 250, 310, and 370 °C, respectively. HOF-102 was exposed to different organic solvents, concentrated acid solutions, boiling water, PBS buffer, and aqueous solutions. The PXRD and the N_2 isotherm measurements after particular treatment showed that HOF-102 maintained its crystallinity, implying that the stability of 2D HOFs could be effectively improved by intermolecular π–π interactions. Therefore, co-planar π-conjugated large aromatic molecules, combining hydrogen bonding and coordinated π–π stacking interaction, are proven to be a good choice for constructing stable HOF materials.

2.1.4 Avoiding the formation of a D/A structure. The residual hydrogen donors/acceptors after self-assembly should be removed because the unpaired hydrogen acceptors/donors may interact with the solvent molecules, this introduces additional difficulty and complexity to the activation process, causing the framework to collapse. In this regard, if allowed, solvents with relatively weak polarity and low boiling points should be used as much as possible, *e.g.*, weak polar solvents such as tetrahydrofuran, dimethyl ether, isopropanol, and others, have been used to prepare highly stable HOFs.[72–74] This kind of HOFs can enable the removal of most of the solvent molecules at room temperature while ensuring the framework's integrity. Hence, avoiding the formation of a D/A structure is a good choice for building stable HOFs.

2.1.5 Others. Introducing proper interpenetration into the structure of HOFs is also an effective means to improve stability. As already well established, interpenetration may improve the physical stability of the framework, impart flexibility and dynamic characteristics, and finely tune the pore environment. Moreover, the interpenetration framework has lower energy and thermodynamic advantages. The ''interpenetrating isomerism'' in 3D HOFs was reported for the first time by Stoddart and coworkers.[75]

In short, the construction of stable HOFs still requires coordination of the strategies mentioned above, *i.e.*, combining a directional H-bond building unit with the rigid organic backbone of co-planar π-conjugated large aromatic molecules. This may yield highly porous HOFs with strong intermolecular interactions and permanent porosity, putting forward an effective solution for constructing HOFs with high stability and permanent porosity in the future.

2.2 Synthons for designing HOFs

In terms of achieving hydrogen bonding, some basic hydrogen bonding synthesizer motifs have been used to design HOFs. So far, many typical building blocks of HOFs have been reported, including diaminotriazine (DAT), carboxylic acid (–COOH), sulfonic acid (–SO_3H), pyrazolre, imidazole, pyridine, and urea (Table 1). It should be noted that these organic groups are not assembled into single crystals but into many polymorphs due to the flexibility of hydrogen bonds. In response to this problem, Cooper and Day *et al.* cleverly used energy–structure–function (ESF) maps of the crystal structure to identify highly porous HOFs with high performance.[76–78]

2.2.1 Diaminotriazine (DAT). DAT and its derivatives, which can serve as hydrogen bond acceptors or hydrogen bond donors, enabled the formation of multiple N–H·bonds (type-1, type-2, and type-3) (Fig. 3a) by self-assembly induced by solvent evaporation. The residual amino groups sequentially formed hydrogen bonds with other DAT or solvent molecules to yield 2D or 3D HOFs (Fig. 3a).[79,80] A series of HOFs were synthesized using DAT building blocks, and the used molecular formula is shown in Fig. 3b. In 1997, Wuest and co-workers reported the first porous HOF that adopted DAT as the building block.[81] After that, a 3D microporous HOF (termed as HOF-1) with permanent porosity was synthesized by incorporating DAT into the backbone.[82] The specific surface area of HOF-1 was 359 $m^2\ g^{-1}$, exhibiting a one-dimensional channel with a hole diameter of ~8.2 Å along the *c*-axis. This inspired the synthesis of a series of microporous HOFs (denoted as HOF-2, HOF-3, HOF-4, HOF-5, HOF-6, HOF-7, HOF-9, and HOF-10) based on DAT.[42,45,50,66,73,83–85] Unbelievably, in 2019, a universal DAT derivative was selected as a hydrogen bond building unit. The first HOF membrane was prepared by a simple solution treatment method, named UPC-HOF-6-120.[86] In the future, various DAT pattern scaffolds may be used to synthesize porous HOFs with different structures and functions.

2.2.2 Carboxylic acid (–COOH). Monomers containing carboxyl function groups are common motifs to form HOFs. Carboxyl groups self-assemble in solution to form hydrogen bonds (O–H···O) (Fig. 4). According to the detailed analysis of the crystal structure by the Cambridge Structural Database (CSD), O–H···O interactions from nearly 140 000 structures show an average bonding distance of 2.77 Å. A shorter bonding

Table 1 Summary of porosity and functionality in porous HOFs

H-Bbonding motifs	HOFs	Solvent	Anti-solvent	Application	Ref.
DAT	HOF-1a	Formic acid dioxane	Dioxane	C_2H_2/C_2H_4 separation	82
	HOF-2a	Methyl ether	—	Enantioselective separation of secondary alcohols	73
	HOF-3a	DMSO	THF	C_2H_2/CO_2 separation	66
	HOF-4	DMSO	—	C_2H_4/C_2H_6 separation	42
	HOF-5a	DMF/DMSO	THF	C_2H_2/CH_4, CO_2/CH_4, CO_2/N_2 separation	45
	HOF-6a	DMF	THF	CO_2/N_2 separation and proton conduction	83
	HOF-7a	DMF	THF	CO_2/N_2 separation and proton conduction.	84
	HOF-9a	DMF/H_2O	—	Selective recognition towards Py over BTX	85
	HOF-10a	DMF/DMSO	THF	Fluorescence Ag^+ sensing	50
	UPC-HOF-6-120	DMSO	Methanol	HOF films for H_2/N_2 separation	86
Carboxylic acid	HOF-BTB	MeOH	—	C2/CH_4 separation	39
	HOF-76a	DMSO	Acetone	C_2H_4/C_2H_6 selective separation	41
	HOF-11a	THF	Hexane	C_2H_2/CH_4, CO_2/CH_4, CO_2/N_2 separation	72
	CPHAT-1a	DMF	—	Fluorescence	88
	PFC-1	DMF	Acetone	Photodynamic therapy	90
	PFC-2	DMF/EtOH	—	C2/CH_4 separation	40
	CBPHAT-1a	DMF	—	Anisotropic fluorescence emission, acid-induced color change	91
	HOF-12	THF/DME	*n*-Hexane	CO_2 adsorption	92
	ABTPA-2	THF	Acetone	CH_4 adsorption	93
	CPDBC-1a	DMF	—	Photoconductivity	94
	Ex-apo	DMF	—	Vapor sorption of hydrocarbons	95
	HOF-TCBP	DMF	—	C4/CH_4, C3/CH_4 separation	89
	HOF-20	DMSO	CH_2Cl_2	Fluorescence sensing of aniline	53
	nano-PFC-1	DMF	—	Electrochromic film	107
	PFC-33	DMA/MeOH	—	Biological antibacterial	108
	PFC-11	EtOH	—	Stepwise adsorption	74
	PFC-12	Isopropanol	—	Stepwise adsorption	74
	PFC-13	EtOH/H_2O	—	Stepwise adsorption	74
Sulfonic acid	HOF-GS-10	MeOH	Acetone	Proton-conducting	46
	HOF-GS-11	MeOH	*p*-Xylene	Proton-conducting	46
	KUF-1	MeOH	Acetone	IV NH_3 adsorption	100
Others	POSS-T_8A	MeOH	—	Metal-ion sensing	49
	PhTCz-1	CH_2Cl_2/EAC	—	Ultralong	51
	PhTCz-2	EtOH/DMF	—	Phosphorescence	51
	HOF-FJU-4	$CHCl_3$/*n*-hexane	—	Micro-lasers	102
	HOF-FJU-5		—		102
	HOF-FJU-1	DMF	—	C_2H_2/C_2H_4 separation	104

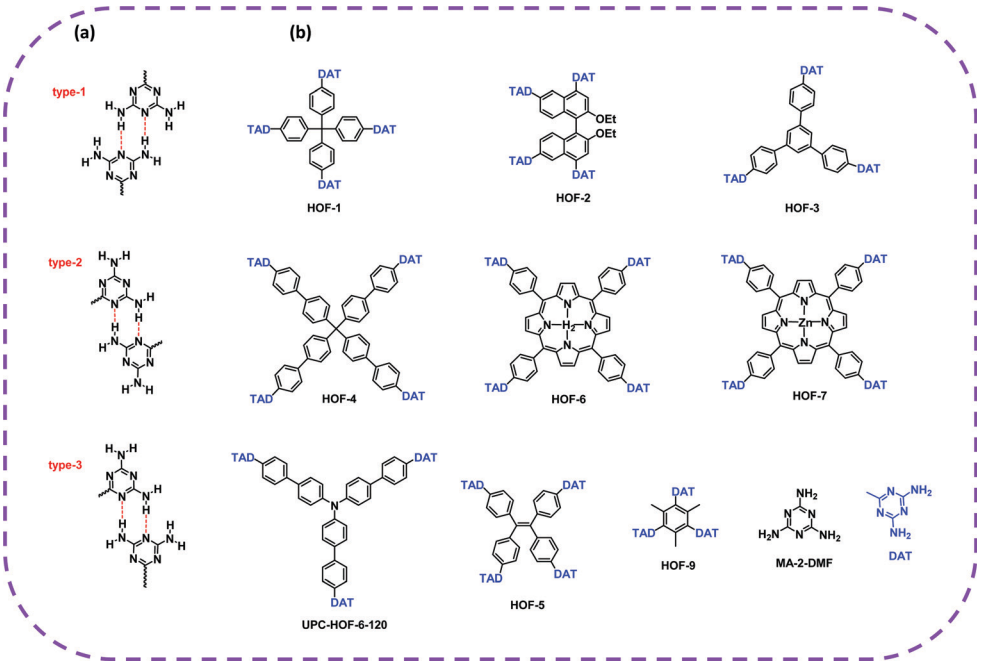

Fig. 3 (a) Supramolecular synthons of DAT moieties. (b) Building units with DAT moieties to form HOFs.

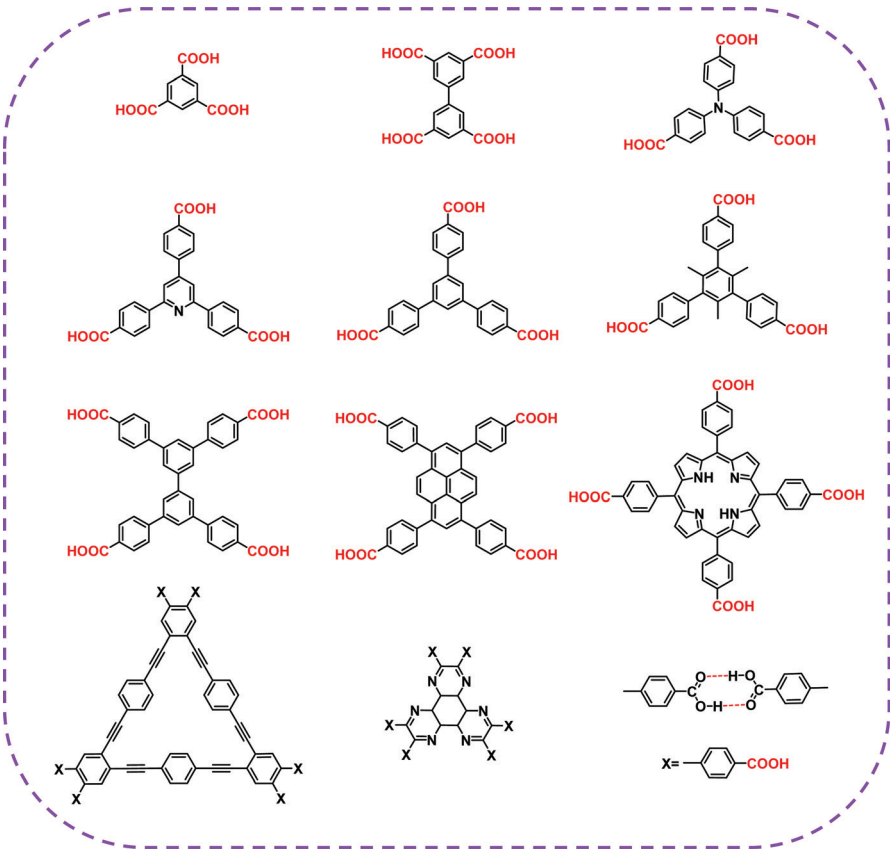

Fig. 4 H-Bond pattern of carboxyl group and unit of formation of HOFs of carboxyl group in the literature.

distance implies stronger hydrogen bond interaction and better orientation. From rational design, a high degree of directivity and strong hydrogen bond interaction can help simplify the chemical reaction for the expanded network of organic

molecular self-assembly. In 2015, Zentner *et al.* used 1,3,5-tris-(4-carboxyphenyl)benzene as a building block self-assembled to form a permanent porous HOF with a BET surface area of 1095 $m^2\ g^{-1}$ and an average pore diameter of 18.5 Å.[87] In 2017, Yang *et al.* prepared a 3D robust HOF, named HOF-11 (1D channels with a pore size of $\sim 6.2 \times 6.8$ $Å^2$).[72] In the same year, Hisaki *et al.* and Hu *et al.* also prepared excellent HOFs.[88,89] In 2018, Yin *et al.* reported a highly stable HOFs, called PFC-1, in which 1,3,6,8-tetra(*p*-benzoic acid)pyrene (H_4TBAPy) was selected as a monomer.[90] PFC-1 exhibited a specific BET surface area of 2122 $m^2\ g^{-1}$ and retained its structural integrity after being immersed in a concentrated hydrochloric acid solution for at least 117 days. Hisaki *et al.* also selected HAT derivatives (CBPHAT) to synthesize porous HOFs with high stability and a BET surface area of up to 1288 $m^2\ g^{-1}$.[91] Subsequently, more researchers chose suitable carboxyl groups as hydrogen bond building units and prepared a series of different HOFs.[53,74,92–95] Conclusively, H-bond interaction and strong π–π interaction formed by carboxylic acid-based building elements have been broadly applied in constructing HOF networks.

2.2.3 Sulfonic acid (–SO_3H). Similarly, ionic charge strengthens the electrostatic properties of hydrogen bonds, so charge-assisted hydrogen bonds can outperform weak hydrogen bond interactions, thereby forming highly stable HOFs (Fig. 5c).[96] In 1994, Etter and Ward first discovered molecular crystals based on hydrogen bonds (N–H···O) between charge-assisted guanidine and sulfonate. The average bonding distance of N–H···O interaction in nearly 120 000 structures is 2.88 Å. Thus, sulfonate was considered to be an ideal material for building charge networks.[97,98] Later, in 2015, Liu *et al.* reported that guanidinium-sulfonate (GS) topologies could be used to enhance H-bond stability.[99] In 2016, Karmakar *et al.* chose disulfonate and guanidine salt ions as building blocks to fabricate hydrogen bonds. The solvent-induced self-assembly method was used to synthesize proton-conducting porous HOFs, named HOF-GS-10 and HOF-GS-11.[46] In 2019, Kang *et al.* dissolved H_4SPM (tetrakis(4-sulfophenly) methane) and Gua-HCl (guanidine hydrochloride) in a mixed solvent of methanol and acetone, which slowly diffused through dichloromethane (CH_2Cl_2) vapor into the mixed solvent leading to the formation of HOFs (named KUF-1) in the solution, with prominent adsorption properties (Fig. 5b).[100] The mechanism of the hydrogen bond formation between sulfonic acid and guanidine salt, and the case where it can evolve into three-dimensional (3D)

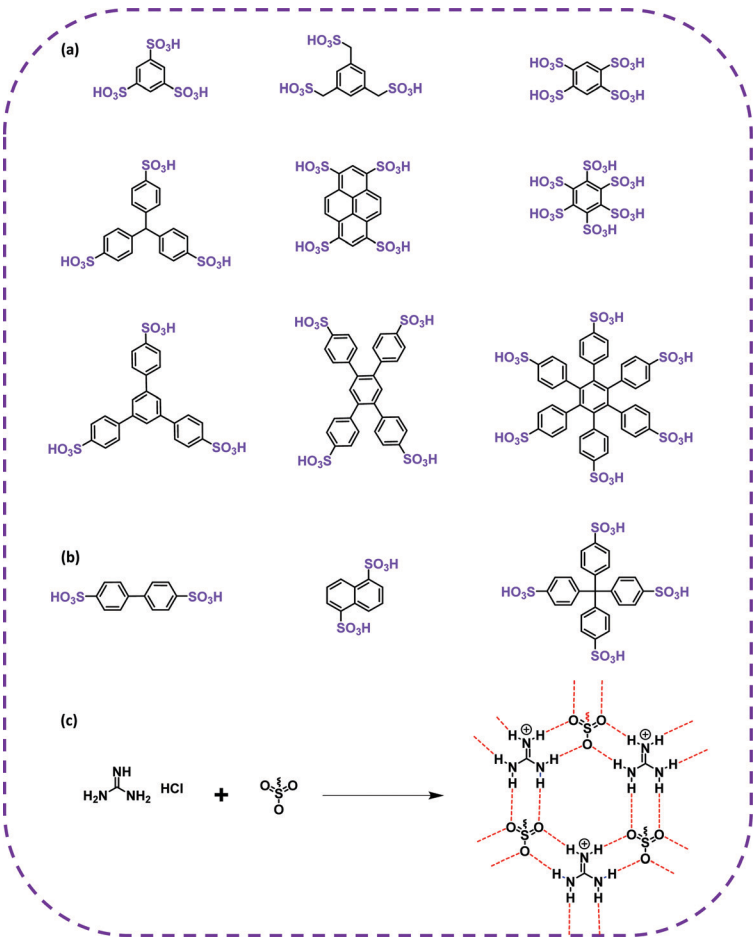

Fig. 5 (a) Sulfonic acid topology that can form hydrogen bonds. (b) The sulfonic acid structure already used to form HOFs. (c) Schematic diagram of hydrogen bond between sulfonic acid and guanidine.

HOFs, has been explored in the literature, but there are still serious uncertainties (Fig. 5a). The unstable sulfonic acid mostly exists in the form of sodium salt, and guanidine salt is guanidine hydrochloride. Therefore, NaCl crystals also form along with the formation of HOFs, affecting the crystal quality of HOFs. Although the previously reported literature focusing on the effect of sodium and guanidine salts on constructing HOFs provided a certain direction, further systematic research is certainly needed.

2.2.4 Others. Some heterocycles can also form hydrogen-bonded supramolecular synthons, so they are also typical building blocks of HOFs (Fig. 6). Importantly, a series of HOFs with heterocyclic hydrogen-bonded supramolecular synthons were reported.[49,51,101] For instance, in 2021, tetraphenylethylene (TPE) was chosen as the main chain for the synthesis of HOFs by Zhao and co-workers. As hydrogen bond acceptors, cyano groups can connect adjacent building blocks through intermolecular hydrogen bonds to form two kinds of porous framework, termed as HOF-FJU-4 and HOF-FJU-5.[102] In HOF-FJU-4, the building blocks are connected with four neighboring blocks by C–N···H hydrogen bonds, and the layers are further superimposed along the *a*-axis *via* the C–H···π interaction. On the contrary, in HOF-FJU-5, the building blocks are connected with two building block molecules by C–N···H hydrogen bonds, and the layers are further superimposed along the *b*-axis *via* C–H···π interaction. Therefore, heterocyclic hydrogen bond supramolecular synthons provide a new way for the development of HOFs.

In conclusion, as long as the synthesizer meets the IUPAC definition,[103] it can be used as a building block for HOFs. The huge synthetic sub-group provides new possibilities for the development of HOFs with different structures and functions.

2.3 Synthetic method

HOFs are a kind of solvated crystals that crystallize slowly in a solvent. However, the crystallization of HOFs is easily affected by precursor concentration, reaction time, temperature, and other factors. Therefore, most of the HOFs are polymorphs. In theory, kinetic isomers can be produced by crystallization at higher concentrations or at shorter reaction times. However, slowing down the crystallization rate or increasing the heat energy can be a straightforward solution to obtain a thermodynamically stable phase. Herein, various methods for synthesizing HOFs are summarized, like liquid/vapor diffusion, evaporation/cooling, electrophoretic deposition, and others.

2.3.1 Liquid/vapor diffusion. The liquid/vapor diffusion can induce the self-assembly of molecules and nanoparticles to form one-dimensional nanomaterials or ordered structures. Lately, the method has been widely applied to synthesize various complex, regular, and ordered porous materials and HOFs. In 2019, Kang *et al.* dissolved H_4SPM (tetrakis(4-sulfophenly)methane) and Gua-HCl (guanidine hydrochloride) in a mixed solvent of methanol and acetone, which slowly diffused through dichloromethane (CH_2Cl_2) vapor into the mixed solvent leading to the formation of HOFs (named KUF-1) in the solution after a few days.[100] The formation of KUF-1 shows that under the synergistic effect of solvent and saturated steam, the crystal nucleation rate can be reduced. The slower the crystal nucleation rate, the higher the crystal quality.

2.3.2 Evaporation/cooling. Evaporation/cooling involves heating the solvent to the boiling point and slowly cooling it down to room temperature. When the solvent reaches the boiling point, heat energy is increased, which is conducive to the formation of thermodynamic phases. Yang *et al.* in 2021 used this method to prepare a HOF suitable for single-crystal

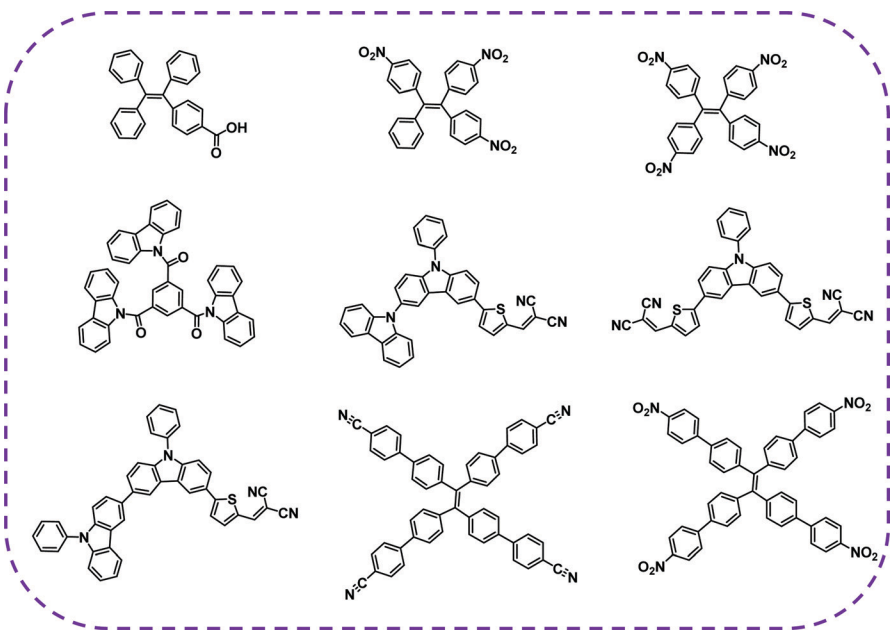

Fig. 6 Some of the heterocyclic structural formulae that form HOFs in the literature.

X-ray diffraction, which was denoted as HOF-FJU-1.[104] They used a protic DMF solvent and, at the same time, the cyano group in the hydrogen bond synthon acted as a hydrogen bond acceptor. The organic building blocks were dissolved in DMF under heating. The resulting solution was cooled down to room temperature, and high-quality crystals were obtained after 12 hours. The obtained HOF-FJU-1 exhibited good stability, and PXRD analysis indicated a pure HOF-FJU-1 phase. In addition, Zhai and co-workers also used this method to prepare water-stable 2D HOFs.[105] This completely demonstrated that the evaporation/cooling method is suitable for the growth of HOFs. This means that increasing the heat energy facilitated the reaction shifting in the positive direction to provide new insight into obtaining high-quality thermodynamic phases.

2.3.3 Electrophoretic deposition. Electrophoretic deposition (EPD) is the most commonly used method for the preparation of thin-film HOFs. EPD is a two-electrode system, the negative electrode is a zinc plate, and the positive electrode is generally FTO conductive glass (it can also be a zinc plate). The EPD device is simple, cost-effective, and suitable for samples with various properties and sizes. More importantly, under the action of an external electric field, EPD can form a uniform and dense film in just a few minutes. Feng *et al.* applied an external voltage to the zinc anode and prepared a uniform thin film in only two minutes based on the EPD discovery.[106] Changing the applied potential from 15 to 90 V yielded a film thickness ranging from 3.8 to 10 μm. In addition, another HOF film was prepared using this method, denoted as nano-PFC-1.[107] Thin-film HOFs prepared by the EPD method pointed out a new direction for the construction of multifunctional HOFs.

2.3.4 Others. The template method is also a common method for preparing thin-film HOFs. The first flexible free-standing membrane was prepared in 2020, denoted as polyHOF.[108] First, the oligomer AA-PEG-AA with two olefin groups was dissolved in isopropanol to form a transparent solution, and then HOF-olefin particles were added, followed by an ultrasonic treatment to obtain a uniformly dispersed suspension. Second, the BDK photoinitiator was added to the suspension and sonicated in the dark for treatment. Third, the turbid liquid was carefully poured into a disc. Finally, under ultraviolet light irradiation, HOF-olefin particles and AA-PEG-AA monomer were copolymerized and cross-linked to form a flexible self-supporting film.

In summary, the crystallization of HOFs is susceptible to changes in solvents, templates, concentration, and temperature, yielding different polymorphs. Therefore, the synthesis conditions and methods should be controlled as much as possible to obtain a single crystal form. Theoretically, slowing down the nucleation rate or the synthesis in a hot solvent is beneficial to the growth of HOFs crystals. The application of liquid/vapor diffusion and evaporation/cooling methods represents progress in this domain, providing a workable approach to assemble stable HOFs. At the same time, it is also pointed out that EPD is the most commonly used method for preparing thin-film HOFs.

3. Applications based on HOFs

3.1 Gas separation and adsorption

Most HOFs are considered a new type of porous media that can adsorb and separate gas molecules due to their permanent pores and self-repairing capacity. In particular, HOFs are fabricated with controlled structures composed of light elements (such as C, H, O, and N) by crystal engineering, and have a low skeleton density, high specific surface area, and permanent pores. The closed cavities in HOFs are suitable for capturing or encapsulating gas molecules, such as O_2, H_2, N_2, CO_2, NH_3, light hydrocarbon mixtures (CH_4, C_2H_2, C_2H_4, and C_2H_6), and the like. Therefore, HOFs have broad application prospects in gas separation and storage.

3.1.1 Hydrocarbon separation. Light hydrocarbons are the best candidate materials for alternative energy and chemical raw materials. In particular, C2 light hydrocarbons, including C_2H_2, C_2H_4, and C_2H_6, are considered the lifeblood of the chemical industry, and they are extensively used in the synthesis of a variety of industrial products ubiquitous to human life, such as fibers, plastics, rubber, and others.[109–111] The hydrocarbon separation requires high energy consumption and harsh operating conditions, such as high pressure and low temperature. Hence, there is an urgent need to develop a separation technology that requires mild operating and energy-saving conditions. At present, using porous materials for adsorption and separation of hydrocarbons is a simple, eco-friendly, and mature approach.[112–114]

HOFs have been extensively used in adsorption separation. More particularly, HOFs are regarded as green separation materials for separating C2 light hydrocarbons (as shown in Table 2), having great developmental potential and broad application prospects. In 2011, Chen and co-workers synthesized the first 3D microporous HOF with permanent pores based on organic monomers with four diaminotriazines, which could selectively separate C_2H_2/C_2H_4 under environmental conditions (Fig. 7a and b).[82] The CO_2 adsorption isotherm at 196 K showed that HOF-1a exhibited permanent porosity (Fig. 7c), which together with structural flexibility of HOF-1a, stimulated the interest in studying its gas separation capabilities,

Table 2 Summary of the absorption capacity of HOFs for hydrocarbons

	C_2H_2		C_2H_4		C_2H_6			
HOFs	273 K	298 K	273 K	298 K	295 K	296 K	298 K	Ref.
SOF-1a	61	50	—	—	—	—	—	37
HOF-BTB	110.3	64.3	85.3[a]	55.7[a]	47[c]	—	—	39
PFC-2	76.3	48	62.2	42.6	—	—	—	40
PFC-1	48	28	—	—	—	—	—	91
HOF-76a	—	—	—	—	—	66.1[c]	—	41
HOF-4a	—	—	17.3[b]	11.1[b]	5.1	3.6	—	42
HOF-5a	182[a]	102[a]	—	—	—	—	—	45
HOF-1a	63[a]	55[a]	8.3[b]	2[b]	—	—	—	82
HOF-3a	58[a]	47[a]	—	—	—	—	—	66
HOF-11a	74[a]	45[a]	—	—	—	—	—	72
HOF-TCBP	—	35[b]	—	32[a]	—	—	—	89
ZJU-HOF-1	—	—	—	39.1	—	—	88[c]	116

[a] Examined at 296 K. [b] Examined at 295 K. [c] At 0.5 bar and RT.

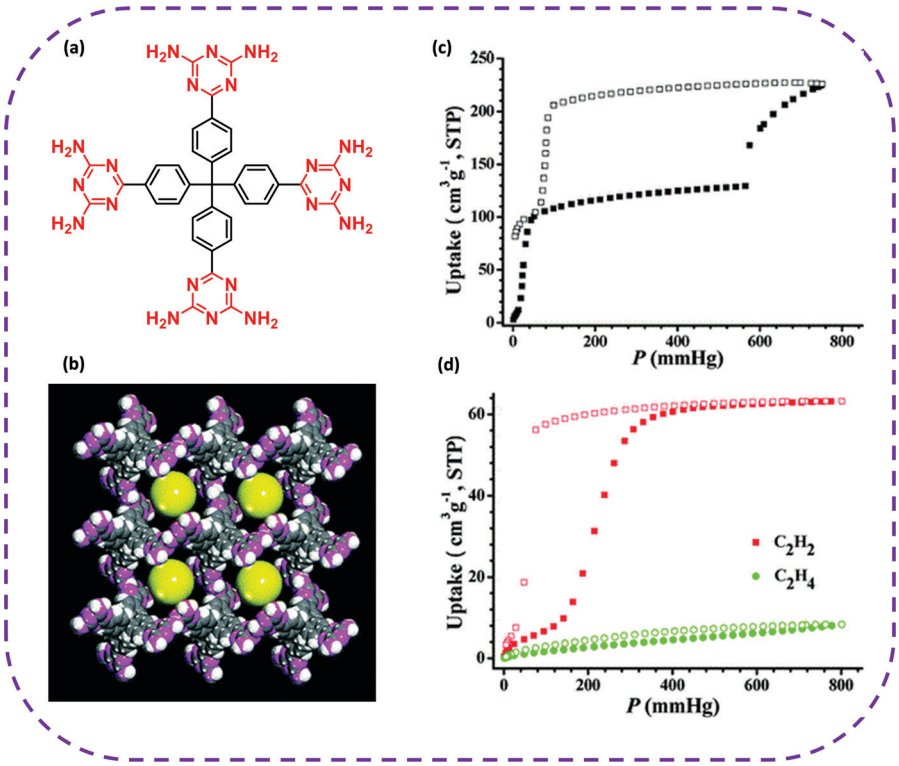

Fig. 7 (a) Construction of the hydrogen-bonded organic unit of HOF-1. (b) X-ray crystal structure of HOF-1 featuring one-dimensional channels along the *c* axis with a size of ~8.2 Å (yellow spheres) and three-dimensional body-centered cubic network topology. (c) CO_2 sorption isotherm at 196 K. (d) C_2H_2 and C_2H_4 sorption isotherms at 273 K. Reproduced with permission from ref. 82. Copyright 2011 American Chemical Society.

especially the separation of C_2H_2/C_2H_4 at ambient temperature. At 273 K, the adsorption capacity of HOF-1a for C_2H_2 was 63.2 $cm^3\ g^{-1}$ (STP), that is, 1 mol HOF-1a adsorbed 2.1 mol C_2H_2 (Fig. 7d), while HOF-1a could only adsorb 8.3 $cm^3\ g^{-1}$ (STP) of C_2H_4 at 1 atmosphere. Therefore, at 273 K, the separation selectivity of C_2H_2/C_2H_4 in HOF-1a was 7.6, while Henry separation selectivity reached 19.3. At 296 K, the selectivity of C_2H_2/C_2H_4 further increased to 14.6.

In 2019, Cao and co-workers constructed a new 3D HOF from 1,3,6,8-tetrakis(*p*-benzoic acid) pyrene (H_4TBAPy), denoted as PFC-2, having a hierarchical mesopores-microporous structure (Fig. 8a and b).[40] The porous framework structure of PFC-2 exhibited two kinds of rhomboid channels with pore sizes of 29.7 and 10.7 Å, respectively (Fig. 8b). The N_2 adsorption–desorption isotherm proved the existence of mesopores in PFC-2 (Fig. 8c). Compared with the reported HOFs, PFC-2 exhibited the largest open channel and highly selective separation of acetylene, ethylene, and methane under ambient conditions (Fig. 7d). The adsorption capacity of C_2H_2 decreased from 76.3 to 47.9 $cm^3\ g^{-1}$ when the temperature increased from 273 to 298 K. As for the C_2H_4 adsorption, when the temperature increased from 273 to 298 K, the adsorption capacity decreased from 62.2 to 41.1 $cm^3\ g^{-1}$. In summary, the highly selective separation of light hydrocarbons by mesoporous PFC-2 provides a practical solution for the design and application of mesoporous HOFs.

Ethane/ethylene (C_2H_6/C_2H_4) separation is always a critical point in the chemical industry.[115] However, developing an efficient, cost-effective separation method still faces many challenges. With the emergence and development of HOF materials, some of the problems have been gradually solved. In 2020, Chen and co-workers skillfully designed a C_6-symmetric organic ligand with six carboxylic acid groups, hexa(4-carboxyphenylethynyl)benzene (HCEB),[41] which was used as a hydrogen bond building unit to construct a new HOF, termed as HOF-76 (Fig. 9a and b). HOF-76 exhibited a one-dimensional triangular channel-like pore with a diameter of 7.0 Å (Fig. 9c). Interestingly, the non-polar/inert pore surface in activated HOF-76a caused the prevalent adsorption of C_2H_6 over C_2H_4, and its separation performance was much higher than that of most reported MOF materials. HOF-76a exhibited a higher separation selectivity to C_2H_6 and C_2H_4 than most developed MOFs and HOF-BTB (1.4).[39] However, the one-dimensional pore size was relatively large, and the lack of strong C_2H_6 adsorption sites yielded poor C_2H_6 absorption, which greatly hindered the reaction yield of the required C_2H_4 products.

Therefore, in 2021, TMBTI was selected as a building block, and colorless stick-like crystals were obtained by vapor diffusion at ambient temperature, denoted as ZJU-HOF-1.[116] The ZJU-HOF-1 framework is more flexible, and reversible solid-state transitions may emerge, which in turn could yield a unique rod-shaped filled desolvated framework (Fig. 10a). The activated ZJU-HOF-1 demonstrated a specific surface area of 1465 $m^2\ g^{-1}$ and a cavity size of 4.6 Å. Remarkably, activated ZJU-HOF-1 exhibited a high BET surface area and optimally

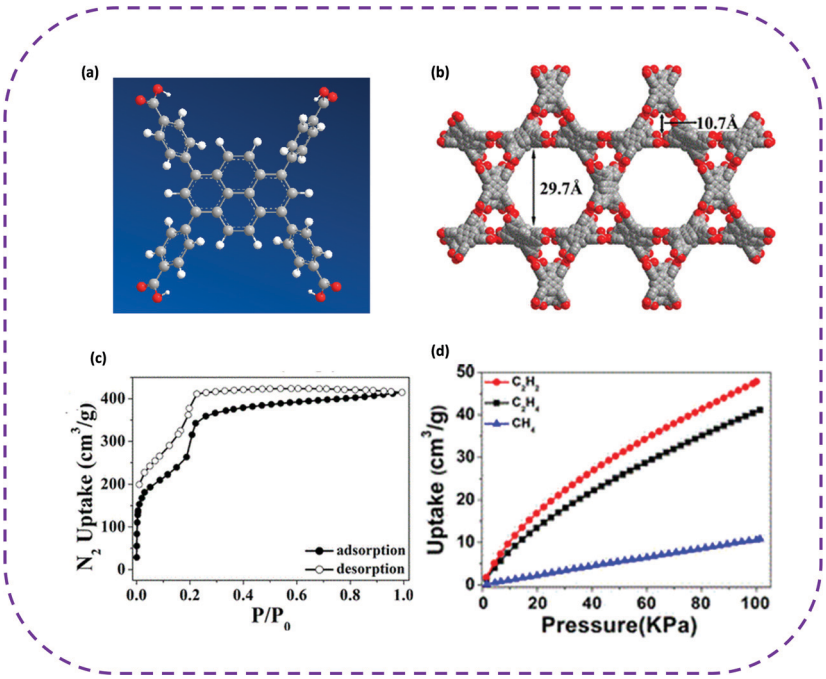

Fig. 8 (a) To construct the molecular structure of PFC-2. (b) The porous frame structure of PFC-2 and two kinds of channels. (c) N_2 adsorption–desorption isotherms (77 K) of desolvated PFC-2. (d) CH_4, C_2H_2, and C_2H_4 single component adsorption isotherm of PFC-2 at 298 K. Reproduced from ref. 40. Copyright 2019 American Chemical Society.

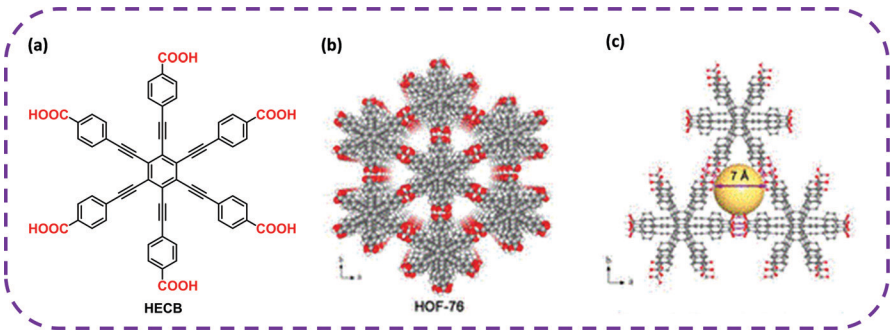

Fig. 9 (a) The organic building block HCEB for the synthesis of HOF-76. (b) The porous frame structure of HOF-76. (c) 1D triangular channel with a diameter of 7.0 Å on the *c*-axis. Reproduced from ref. 41. Copyright 2020 Royal Society of Chemistry.

interacted with C_2H_6, achieving efficient and selective separation of C_2H_4/C_2H_6. The single-component adsorption isotherms indicated that the adsorption of C_2H_6 was significantly better than that of C_2H_4 under the conditions of 273 or 298 K at 1 bar (Fig. 10b). However, on comparing ZJU-HOF-1 and HOF-76a, ZJU-HOF-1 exhibited a steeper C_2H_6 adsorption isotherm in the entire 1 bar range. That is, ZJU-HOF-1 absorbed more C_2H_6 than HOF-76a (Fig. 10c). It is worth noting that when separating and mixing C_2H_6/C_2H_4 (50/50, v/v), the adsorption capacity of ZJU-HOF-1 for C_2H_6 (88 $cm^3\ g^{-1}$ at 298 K) was 2.3 times higher than that of HOF-76 (38 $cm^3\ g^{-1}$) (Fig. 10d). This unique pore structure of ZJU-HOF-1 enabled a high C_2H_6 absorption rate and high selectivity to C_2H_6/C_2H_4 (2.25). In short, the examples of C_2H_6/C_2H_4 separation reported above may guide future porous HOFs to solve important and challenging gas separation problems.

As presented above, porous HOFs play important roles in the separation of industrial hydrocarbons. In this process, the channel confining effect and hydrogen bond interaction seem to control the absorption of different C2 hydrocarbons simultaneously. In the future, the investigation of new types of porous HOF materials can promote the separation of small hydrocarbons.

3.1.2 H_2/N_2 separation. Membrane separation technology has unique characteristics of simple operation, low energy consumption, environmental friendliness, and others. The membrane material lies in the core of membrane separation, attracting research attention from many aspects. Feng *et al.* prepared the first microporous HOF membrane by optimizing the solution processing method, denoted as UPC-HOF-6-120, and used it to separate H_2/N_2.[86] UPC-HOF-6-120 was prepared by two steps. First, a stable, flexible, and porous HOF was

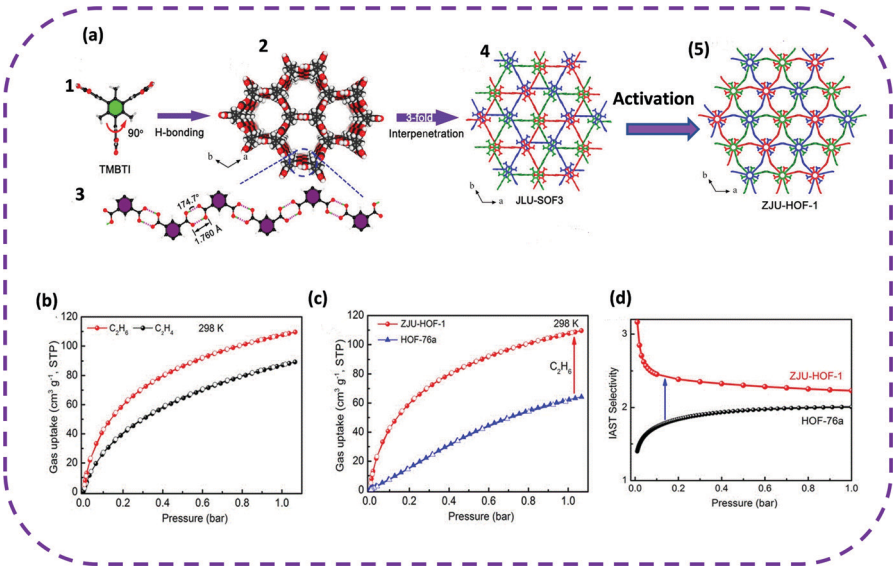

Fig. 10 (a) (1) The structure of TMBTI. (2) A single network constructed using TMBTI molecules. (3) A rod-shaped H bond chain formed using isophthalic acid groups along the *c* axis. (4) Triple interpenetrating structure of JLU-SOF-3. (5) The modeled structure of ZJU-HOF-1 upon activation, revealing an obvious structural transformation between JLU-SOF-3 and ZJU-HOF-1. (b) Adsorption isotherms of C_2H_6 and C_2H_4 for ZJU-HOF-1 at 298 K. (c) Comparison of C_2H_6 adsorption isotherms for ZJU-HOF-1 and HOF-76a at 298 K. (d) C_2H_6/C_2H_4 IAST selectivity of ZJU-HOF-1 as compared with HOF-76a at 298 K. Reproduced from ref. 116. Copyright 2021 Wiley-VCH.

synthesized using organic components based on DAT, named UPC-HOF-6 (Fig. 11a). The smallest channel size of UPC-HOF-6 was about 2.8 Å, which is suitable for separating H_2 from other gases. Second, a continuous UPC-HOF-6-120 membrane was successfully prepared through simple solution treatment using a template method (Fig. 11b). As expected, the UPC-HOF-6-120

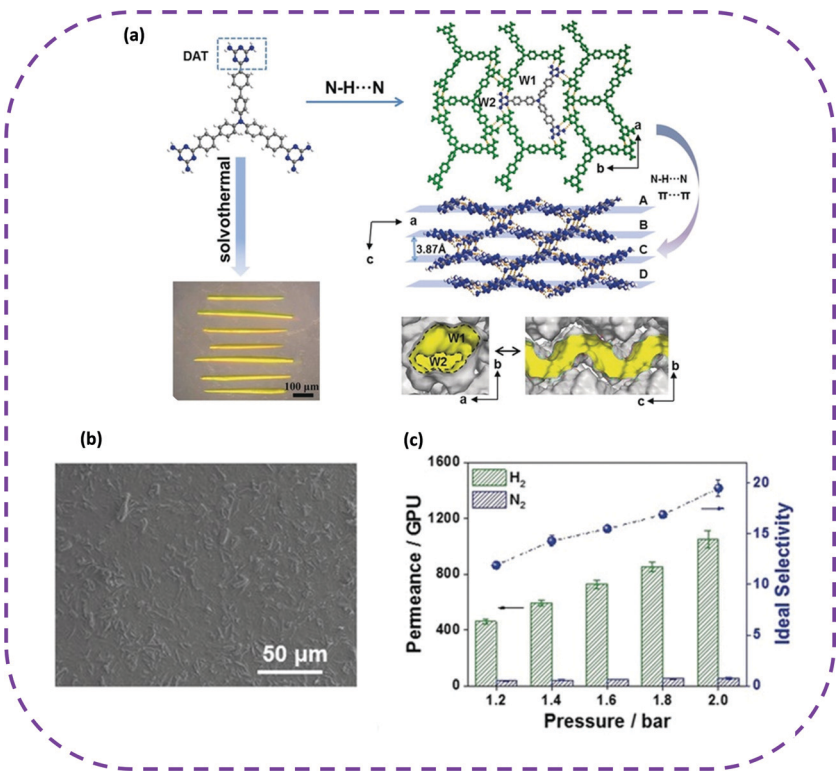

Fig. 11 (a) Organic linker, X-ray crystal structure, and digital photograph of UPC-HOF-6. (b) Top-view SEM image of the UPC-HOF-6-120 membrane. (c) Single gas permeation of the UPC-HOF-6-120 membrane at 25 °C and varied *trans*-membrane pressure drops. Reproduced from ref. 86. Copyright 2020 Wiley-VCH.

membrane exhibited high selectivity for H_2/N_2 separation. More interestingly, H_2 permeability increased significantly with pressure, while N_2 permeability increased only slightly, thereby enhancing H_2/N_2 selectivity (Fig. 11c). The corresponding separation factor increased from 17.2 to 20.5 when the H_2/N_2 ratio increased from equimolar to 3. At the same time, the UPC-HOF-6-120 membrane also exhibited good self-healing properties, that is, the scratched membrane healed easily after the DMSO steam treatment.

As stated above, the excellent pressure-regulated H_2/N_2 separation performance and self-healing ability of the UPC-HOF-6-120 membrane enable the HOF membrane as a potential material for separating multi-component mixtures. The emergence of membrane separation has opened a new door for the future application of HOFs in separation and adsorption.

3.1.3 Carbon dioxide (CO_2) adsorption. CO_2 is a greenhouse gas that causes global warming. According to data analysis, from 1906 to 2015, the Earth's average surface temperature has increased by 0.74 K, and it is expected to continue to increase by 0.3–4.7 K in the 21st century.[117] The increase in the CO_2 content in the atmosphere and the resulting global warming seriously hinder the sustainable development of global ecosystems. Thus, adsorption of CO_2 is a challenging and important research topic at hand. As MOFs and COFs have been widely used in CO_2 adsorption and separation due to their porosity,[118] HOFs also have broad application prospects in this field. In 2020, Li *et al.* reported nearly ideal hexagonal honeycomb motifs, PFC-11 and PFC-12 (Fig. 12a), based on planar H_3TATB molecules (4,4′,4″-(1,3,5-triazine-2,4,6-triyl)tribenzoic acid). These frameworks were expanded into wavy 2D layers, and then microporous HOFs were formed.[74] Further research indicated that PFC-11 and PFC-12 possessed a one-dimensional spiral cavity (Fig. 12b). The CO_2 adsorption capacity of these two porous materials was tested (Fig. 12c), and no stepped adsorption phenomenon appeared on the obtained adsorption isotherm. However, at a pressure of 1 bar, the CO_2 absorption values of PFC-11 were 90.3 and 65.1 $cm^3\ g^{-1}$, respectively, the highest among all reported HOFs. In short, the discovery of this material has raised a new level for the application of HOF materials in CO_2 adsorption.

In summary, HOFs have emerged as the best candidate materials for CO_2 adsorption (Table 3). Interestingly, the pores of HOF materials can be tuned by flexible designing organic groups, thereby accelerating the development of HOF materials as new porous adsorbents.

3.1.4 Ammonia (NH_3) adsorption. Ammonia (NH_3) is a highly toxic gas and an important raw material for manufacturing nitric acid, fertilizers, explosives, and some drugs; thus, it is an irreplaceable chemical substance.[119,120] So far, porous materials, such as MOFs, COFs, and CMPs (conjugated microporous polymers, CMPs), have been widely used as NH_3 adsorbents.[121–124] However, despite their high adsorption capacity, the preparation of these porous materials is complicated, and there is a strong interaction between NH_3 and active acidic sites, which may result in high regeneration temperatures or incomplete regeneration of the materials.[125] Therefore, the most important task at this stage is to develop an ideal type IV adsorbent that can be effectively regenerated under mild conditions, with a great application value for NH_3 adsorption.

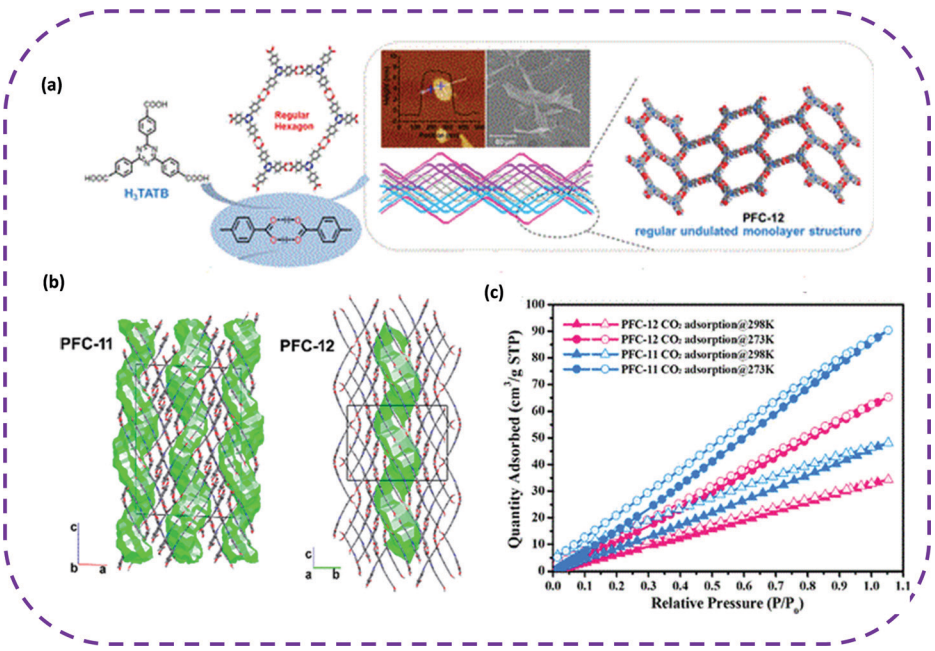

Fig. 12 (a) Representation of the chemical structure, a hexagonal honeycomb pattern obtained by H_3TATB. Atomic force microscope (AFM) and scanning electron microscope (SEM) images of the solute in the supernatant during the crystallization process of PFC-12 (inset) (five and three days, respectively). (b) Crystal structures of PFC-11 and PFC-12 showing the shape of the cavities in green. (c) CO_2 adsorption isotherm of PFC-11 and PFC-12 at 273 and 298 K. Reproduced from ref. 74. Copyright 2020 American Chemical Society.

Table 3 Results of CO_2 uptake by HOFs

HOFs	CO_2 ($cm^3\ g^{-1}$)	Temperature/K	SA_{BET} ($m^2\ g^{-1}$)	Ref.
HOF-8	57.3	196	—	130
HOF-9	40	296	286	85
HOF-11	194	196	687	72
PFC-11	90.3	273	751.3	74

In 2019, Kang *et al.* prepared a beige transparent KUF-1 single crystal based on tetrakis(4-sulfophenyl) methane (H_4SPM) and guanidine hydrochloride (Gua-HCl) in a methanol/acetone mixed solvent (Fig. 13a).[100] This framework encompassed plenty of hydrogen bonds between adjacent sulfonate anion SPM^{4-} pairs and four guanidine cations ($GuaH^+$), in which the O atom of SPM^{4-} can form multiple hydrogen bonds with the NH group of the adjacent $GuaH^+$ (Fig. 13b). The porosity of KUF-1a was fully verified by the gas adsorption isotherms of N_2, H_2, and O_2 of KUF-1a. (Fig. 12c). After that, the NH_3 adsorption isotherms of KUF-1a at three different temperatures were recorded (Fig. 13d). The NH_3 adsorption capacity was 0.97 mmol g^{-1} at 283 K and 1 bar. More interestingly, at 298 K and 0.65 bar, the adsorption capacity of NH_3 was 3.41 mmol g^{-1}, and when pressure reached 1 bar, the adsorption capacity increased to 6.67 mmol g^{-1}. Although the adsorption capacity of NH_3 at 298 K was about 7 times higher than that at 283 K, the adsorption capacity showed a decreasing trend when the temperature reached 313 K. The new HOF showed a unique IV-type isotherm of NH_3. In comparison, this material could be completely regenerated without losing capacity under room temperature and vacuum conditions.

3.1.5 Sulphur dioxide (SO_2) adsorption. Sulfur dioxide (SO_2), the simplest and most common sulfur oxide, is one of the major pollutants in the air. The burning of fossil fuels with a high sulfur content is the main source of SO_2 emission. An excessive SO_2 content may cause serious damage to the environment and harm human health. In addition, SO_2 hinders the adsorption capacity of CO_2 adsorbents, causing catalyst deactivation in methane combustion and nitrogen oxide reduction.[126,127] At present, the most commonly used adsorption method is the washing method, but it cannot completely remove SO_2.[128] Therefore, it is necessary to develop a porous solid adsorbent sensitive to gaseous SO_2 to achieve sustainable development.

In 2019, Jancik and co-workers prepared permanent pores and functional hydrogen bond frameworks (termed as UNAM-1) through the charge-assisted H-bond between $[Cu^{II}Cu^{I}_{12}(HL)_{12}]^{10-}$ and $[Me_2NH_2]^+$ units, and reversibly adsorbed SO_2 (Fig. 14a).[129] In the cubic crystal structure of UNAM-1, $[Cu_{13}(HL)_{12}]^{10-}$ anions interact with DMAH cations (n/n : 1 : 1) through hydrogen bonds (Fig. 14b), and the multiple hydrogen bond interactions in the UNAM-1 structure yield a robust crystal. Consequently, it was unexpectedly discovered that this HOF material was extremely sensitive to capturing highly corrosive acidic SO_2. The adsorption capacity of SO_2 was 1.1 mmol g^{-1} at 0.05 bar, and the obtained adsorption isotherm belonged to type-I. As the pressure increased, the SO_2 adsorption capacity increased in little increments. It is worth noting that the SO_2 adsorption capacity reached 3.5 mmol g^{-1} at 1 bar (Fig. 14c). To our best knowledge, UNAM-1 is the first material that exhibited this reversible SO_2 adsorption. This also highlights the broad prospects of this special material in new applications and points out a new direction for SO_2 adsorption. At the same time, this study also enriches the design strategies of multifunctional HOF materials.

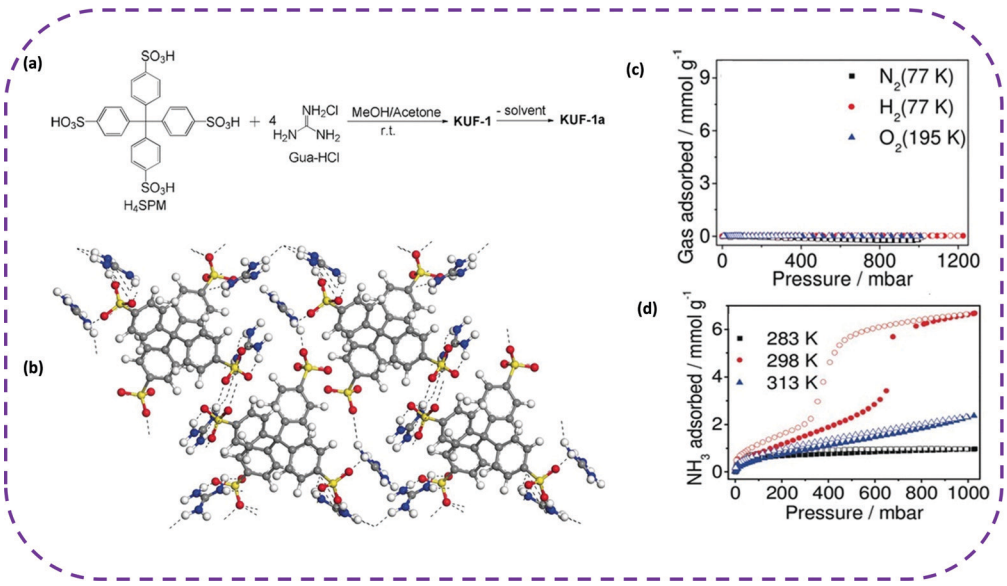

Fig. 13 (a) Synthetic scheme of KUF-1 and KUF-1a. (b) Network structure showing multiple hydrogen bonds (dotted lines) among the NH groups of $GuaH^+$ and the O atoms of SPM^{4-} in KUF-1a. N blue, S yellow, O red, and C gray. (c) Isotherms of N_2, H_2, and O_2 for KUF-1a. (d) NH_3 isotherm of KUF-1a at the indicated temperatures. Filled symbols denote adsorption and open symbols denote desorption. Reproduced from ref. 100. Copyright 2019 Wiley-VCH.

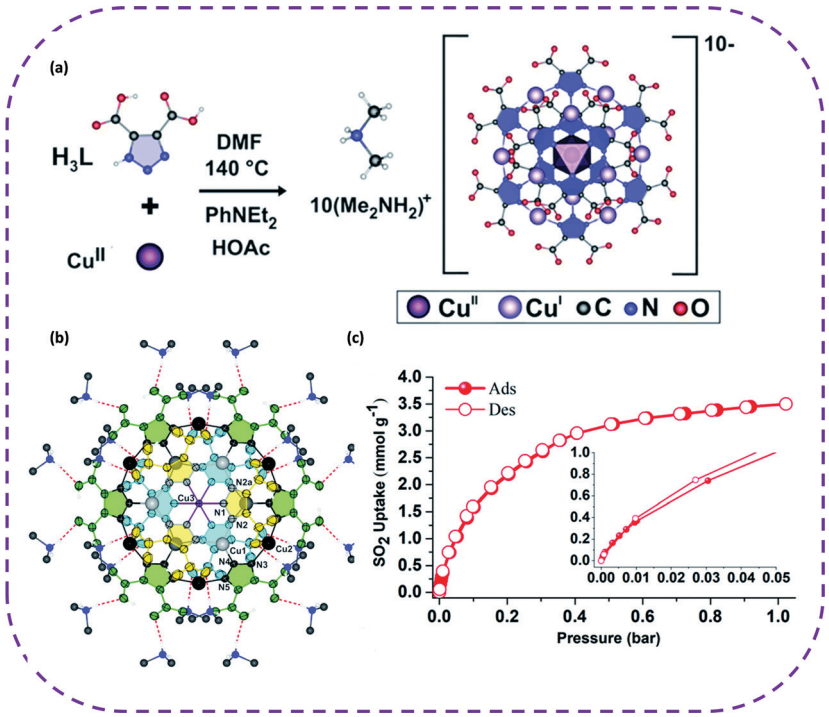

Fig. 14 (a) Schematic diagram of the solvothermal synthesis of UNAM-1. (b) Molecular structure of the $[Cu_{13}(HL)_{12}]^{10-}$ anion (building block of the UNAM-1 framework) with thermal ellipsoids at 50% probability. Hydrogen bonds between dimethylammonium cations and $[Cu_{13}(HL)_{12}]^{10-}$ anion are also depicted as orange dashed bonds. The two CuI atoms are represented as grey and black spheres, respectively. (c) Experimental SO_2 adsorption–desorption isotherm collected for an activated UNAM-1 sample (filled red circles = adsorption; open red circles = desorption) at 35 °C and up to 1 bar. Reproduced with permission from ref. 129. Copyright 2019 Royal Society of Chemistry.

3.1.6 Liquid adsorption. Since the emergence of HOFs, their application in gas adsorption has gained a prominent breakthrough, but there are only a few reports on the adsorption of liquids. Until 2013, the emergence of HOF-8 completely broke the deadlock. HOF-8 was synthesized with an organic unit N1, N3, N5-tris(pyridin-4-yl)benzene-1,3,5-tricarboxamide (TPBTC) as the monomer, in which pyridine N atoms and amide H atoms acted as acceptors and donors of hydrogen bonds, respectively.[130] Each TPBTC molecule is connected to the other three TPBTC molecules *via* hydrogen bonds, creating a 2D supramolecular layer along the *ac* plane (Fig. 15a–c). This layer is stacked by two adjacent layers, forming a 3D microporous HOF (Fig. 15d). The adsorption–desorption test was performed under mild conditions to illustrate the permanent porosity of HOF-8 more convincingly, and unexpected results were obtained (Fig. 15e). The adsorption isotherm that HOF-8d was very sensitive to the selective adsorption of CO_2, but not to N_2 and H_2. At 298 K, the CO_2 adsorption isotherm showed a typical type-I behavior. At 1 bar, the magnitude of CO_2 uptake increased to 57.3 $cm^3\ g^{-1}$ (STP). More interestingly, the activated HOF-8 was extremely sensitive only to liquid benzene. In the ^{13}C NMR spectrum of the benzene-adsorbed activated HOF-8, the ^{13}C resonance peak of the benzene indicator was detected at 128.3 ppm (Fig. 15f). The application of HOF-8 in gas–liquid separation and purification provides an effective method for the preparation of multifunctional HOF materials in the future.

3.2 Proton conduction

Recently, HOFs composed of H-bond connections have emerged as ideal conductive materials since the hydrogen bond donors/acceptors of the building block can be regarded as proton sources or carriers. Furthermore, hydrogen bonds provide a variety of proton transport pathways. The unique properties of HOFs open up new possibilities for membrane manufacturing, thereby enabling a novel production method for solid lightweight proton-conducting electrodes. It is recommended to construct an ionic backbone as a rich source of protons to promote water-mediated proton conduction. Compared with most MOFs, the most attractive fact about HOF conductors is that most HOFs exhibit extremely high stability under different relative humidities, facilitating proton conduction. A permanent porous frame consisting of internal proton carriers was designed to achieve excellent proton conductivity in HOFs.

Porous guanidine sulfonates are good candidates since their ionic backbone acts as a proton source. In 2016, Karmakar *et al.* reported 2D porous HOF materials based on guanidine-containing aromatic sulfonates, named HOF-GS-10 (with guanidinium and 1,5-naphthalenedisulfonate as construction units) and HOF-GS-11 (with guanidinium and 4,40-biphenyldisulfonate as construction units), exhibiting high proton conductivity under humid conditions (Fig. 16a).[46] In HOF-GS-10, oxygen atoms in each disulfonate connect with six adjacent guanidine cations *via* charge assistance, and each guanidine cation is connected to

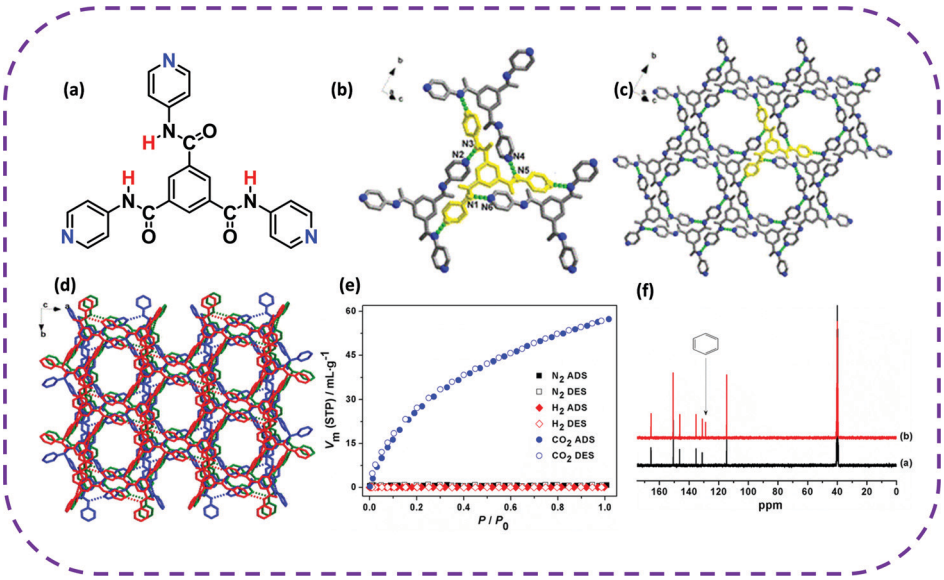

Fig. 15 (a) Molecular structure of TPBTC. (b) Hydrogen-bonding interactions observed in HOF-8. (c) 2D supermolecular layer structure of HOF-8. (d) 3D supermolecular microporous structure of HOF-8. (e) N_2, H_2, and CO_2 sorption isotherms for HOF-8d at 298 K. (f) Partial ^{13}C NMR spectra (400 MHz, 298 K, and DMSO-d_6) of desolvated HOF-8 (black) and HOF-8d with absorbed benzene (red). Reproduced from ref. 130. Copyright 2013 American Chemical Society.

three disulfonates, forming a 2D cellular double-layer network (Fig. 16b). HOF-GS-11 with a double-layer structure similar to HOF-GS-10 has a moving ribbon structure instead of a quasi-hexagonal sheet. The permanent porosity of the two HOFs was verified by the CO_2 adsorption isotherm at 195 K (Fig. 16c). Surprisingly, the study of water adsorption behavior showed that the water absorption of HOF-GS-10 was 3.47 mmol g^{-1}, while the water absorption of HOF-GS-11 reached 11.6 mmol g^{-1}. Given the

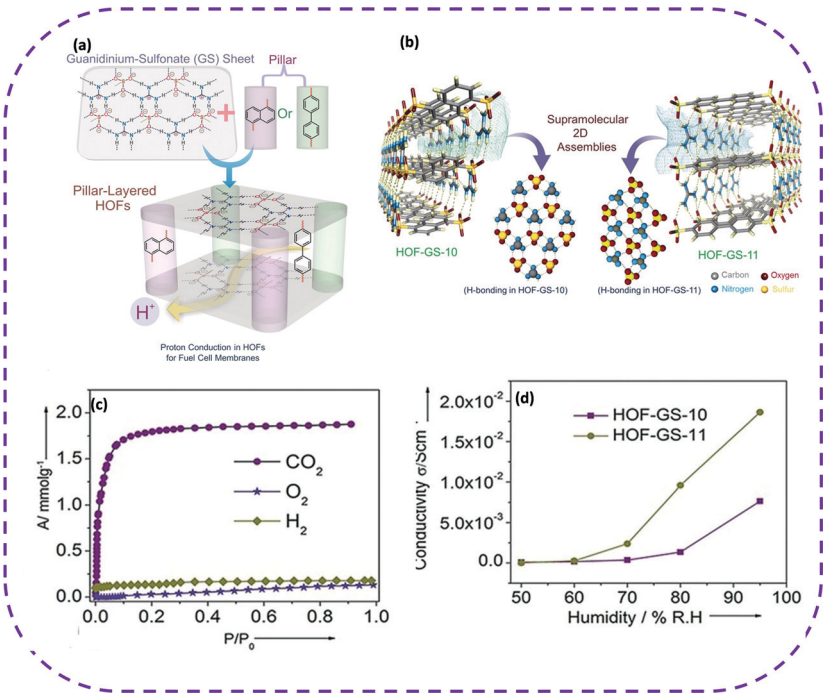

Fig. 16 (a) Schematic representation of hydrogen-bonded frameworks based on arene sulfonates and guanidinium ions showing the proton-conduction pathway. (b) Hydrogen-bonded 2D frameworks of HOF-GS-10 and HOF-GS-11 showing the hydrogen-bonding interaction between the sulfonate groups and the guanidinium cations in both the compounds. (c) CO_2 (dots), O_2 (stars), and H_2 (diamonds) adsorption isotherms of HOF-GS-10 at 195 K (CO_2 and O_2) and at 77K (H_2). (d) Proton conduction values of HOF-GS-10 and HOF-GS-11 at varying humidity and at 30 °C. Reproduced from ref. 46. Copyright 2016 Wiley-VCH.

coherence and porosity of the H-bond network, these two HOFs can be used for solid-state proton conduction under high humidity conditions. Under different relative humidities and temperatures, the proton conductivity of HOF-GS-10 and HOF-GS-11 was significantly different (Fig. 16d). In addition, the activation energy of these compounds was also relatively low, further demonstrating that HOFs are the most promising lightweight materials for fuel cell technology. It is worth noting that HOF materials have made breakthroughs in the application of proton conductivity. Wang *et al.* reported the preparation and proton conductivity of a 3D porous porphyrin-based HOF material [$(NiH_4TPPP)(Me_2NH_2)_4$] (DMF) $(H_2O)_4$ synthesized from nickel phosphate-based porphyrin (NiH_8TPPP), denoted as UPC-H5.[131] The proton conductivity of the crystal was different depending on the relative humidity and temperature. This shows that guest-tuning can improve the proton conductivity of HOF-based materials. This undoubtedly helps the design and development of new HOF-based proton conductors.

In summary, for proton conduction in an aqueous medium, the proton conductivity of HOFs can be compared with high-conductivity MOFs and commercial Nafion membranes. The original pioneering work pointed out the direction for a more in-depth exploration of high-conductivity HOFs, but the exploration of HOFs for proton conduction is still very rare. Low density, high crystal quality, solution processability, and especially high proton carrier ability recommend that HOFs have broad prospects in the future alternative new energy field (Table 4).

Table 4 Summary table of proton conductivity

HOFs	Relative humidity (%)	Temperature (K)	Proton conduction (S cm^{-1})	Ref.
HOF-GS-10	60	303	1.78×10^{-4}	46
HOF-GS-11	60	303	2.6×10^{-4}	
HOF-GS-10	98	300	0.75×10^{-2}	
HOF-GS-11	98	300	1.8×10^{-2}	
UPC-H7	30	313.15	8.79×10^{-4}	47
UPC-H7	40	313.15	1.28×10^{-3}	
UPC-H7	70	313.15	9.21×10^{-3}	
UPC-H8	30	353.15	1.73×10^{-2}	
UPC-H8	60	353.15	3.09×10^{-2}	
UPC-H8	70	353.15	5.59×10^{-2}	
UPC-H9	30	353.15	2.68×10^{-2}	
UPC-H9	60	353.15	4.76×10^{-2}	
UPC-H9	70	353.15	4.62×10^{-2}	
UPC-H5	40	313.15	9.28×10^{-6}	131
UPC-H5	40	353.15	4.68×10^{-5}	
UPC-H5	95	300.15	5.59×10^{-4}	
UPC-H5	95	353.15	1.71×10^{-3}	
UPC-H5	99	353.15	1.85×10^{-3}	
UPC-H5a	40	353.15	5.22×10^{-5}	
UPC-H5a	95	300.15	7.00×10^{-3}	
UPC-H5a	95	353.15	1.82×10^{-2}	
UPC-H5a	99	353.15	3.42×10^{-2}	
UPC-H5a@NH_3H_2O	40	353.15	1.43×10^{-3}	
UPC-H5a@NH_3H_2O	95	300.15	1.47×10^{-2}	
UPC-H5a@NH_3H_2O	95	353.15	8.68×10^{-2}	
UPC-H5a@NH_3H_2O	99	353.15	1.59×10^{-1}	

3.3 Luminescence based applications

HOFs are pure organic materials rationally designed from H-bonded components. Rigid aromatic groups with a large π-conjugated system are usually selected for hydrogen bond construction to obtain porous HOFs with high stability.[132] Such building units are usually fluorescence and phosphorescence dyes, fully demonstrating that HOFs are promising luminescent materials. Luminescent porous materials have been widely used in many fields, such as chemical sensing, fluorescence detection, and biological imaging, owing to their luminescence properties.[133–136] Therefore, HOFs also exhibit great application potential as luminescent materials. It is worth noting that the high crystallinity of HOFs has a highly ordered arrangement of organic chromophores, showing a significantly different emission behavior from that in their solution state. A luminophore is closely contacted between the crystal lattice and certain molecules in the crystalline state, causing a spectral shift, loss of electronic structure, broadening the emission band, and prolonged emission lifetime. At the same time, the involved extensive intermolecular interaction enables effective electronic interaction between the fluorescent groups, which in turn changes the luminescence. Therefore, HOFs show great potential in optical applications.

3.3.1 Sensing and fluorescence detection. Generally, specific recognition of guest molecules always causes variation in the emission spectral variation of host HOFs, yielding the specific sensing of the guest molecules. Hisaki *et al.* used C_3-symmetric π-conjugated planar molecules as building blocks to develop rigid HOFs with permanent pores.[137–141] A typical CPHATN-1a[141] is taken as a representative to briefly describe the research work. CPHATN-1a is a 3D rigid HOF, constructed based on a hexaazanaphthalene derivative (CPHATN). Pyrazine N atoms are differently protonated depending on the pH value. Therefore, CPHATN-1a can be applied for HCl sensing by reversible color changes. For example, after dropping a 37% HCl aqueous solution, CPHATN-1a instantly changed from the original yellow to reddish-brown. By heating the reddish-brown material, as HCl slowly volatilized, the material's original color was gradually restored (Fig. 17a). It is worth noting that acid-sensitive color changes can only be observed in the case of crystalline solvate CPHATN-1. When the HOF crystal is placed in HCl vapor, the absorption and the emission spectra were almost the same (Fig. 17b). As indicated in Fig. 17b, HOFs are extremely sensitive to acid vapor. Interestingly, by exposing to air and ambient temperature for 48 hours, the original absorption and emission spectra could be restored by 90% (Fig. 17c). In addition, CBPHAT-1a[142] and CPBTQ-1a[143] also contain a pyrazine ring in the central core like CPHATN-1a. Therefore, they also have corresponding reversible color changes with a change in the pH value. In short, adding HCl quenches their fluorescence. After the removal of HCl, the emission spectrum is restored. Therefore, HOFs can be used many times as sensors for acidic atmospheres.

In 2020, Chen and co-workers chose aromatic tetracarboxylic acid 5-(2,6-bis(4-carboxyphenyl)pyridin-4-yl)isophthalic acid (H_4BCPIA) as a building unit to form a microporous three-dimensional HOF, named HOF-20.[53] In HOF-20, one H_4BCPIA

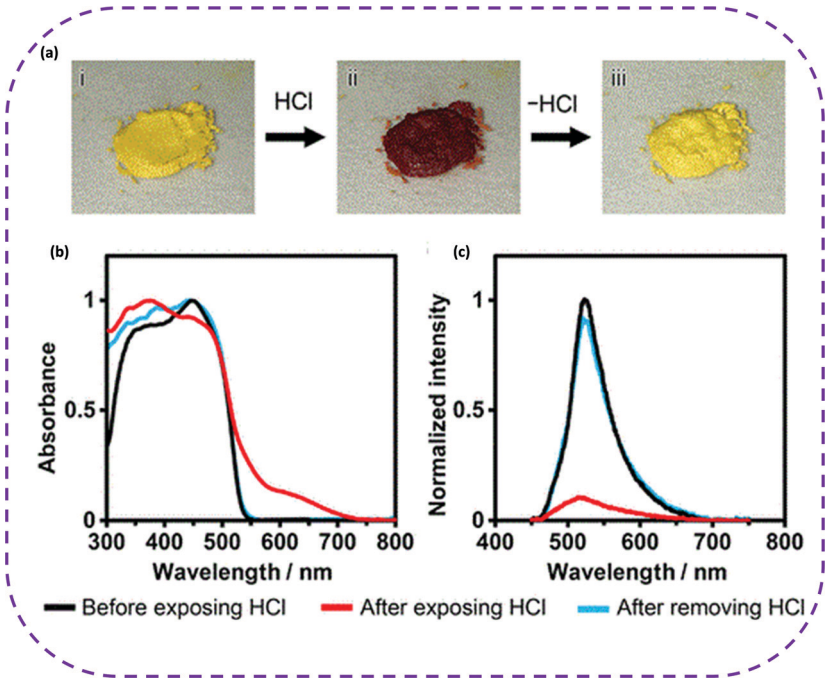

Fig. 17 (a) HCl-responsive color changes of crystalline bulks of CPHATN-1a (i) before exposure, (ii) after 37%-HCl was added, and (iii) after heating at 423 K for 30 min. (b) Absorption and (c) emission spectra of solid CPHATN-1a upon exposure to HCl atmosphere for 40 min and after leaving the exposed crystals in air for 48 h to remove HCl. Reproduced from ref. 141. Copyright 2019 American Chemical Society.

linker can form four pairs of hydrogen bonds and connect with four adjacent linkers (Fig. 18a). The center of H_4BCPIA contains a pyridine ring and a benzene ring, and the C–C bond rotation causes the formation of a twisted tetrahedral conformation (Fig. 18c). Therefore, the constructed HOF-20 exhibited a three-dimensional framework (Fig. 18b and e). HOF-20 possessed a one-dimensional diamond-shaped pore with a pore diameter of 13.0 Å (Fig. 18d). Interestingly, HOF-20 maintained its structural integrity in water, boiling water, and concentrated hydrochloric acid. Due to the high stability of HOF-20 in an aqueous solution, they studied its aniline fluorescence detection ability in water. Incredibly, when aniline (10 μL, 100 mM) was added, the fluorescence intensity of HOF-20 was significantly enhanced, reaching an enhancement efficiency of 142%. Recently, new research progress has been made in the detection of aniline. Zhang and co-workers chose *N*,*N*′-bis(5-isophthalic

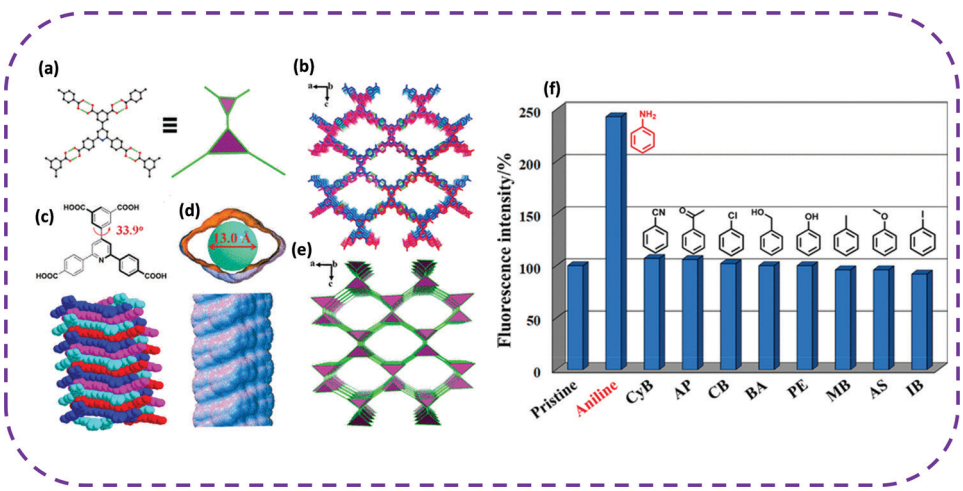

Fig. 18 Crystal structure of HOF-20. (a) View of the connection of adjacent building blocks and simplified two interconnected 3-*c* triangular nodes. (b) Representation of the porous framework. (c) Twisted nonplanar conformation of the H_4BCPIA linker (top) and its shape-fitted 1D stacked pore (bottom). (d) The 1D rhombic pore (top) and visualization of the helical pore surface (bottom) in HOF-20. (e) Augmented $ThSi_2$ net. Color code: C, black; O, red; and N, blue. C-bound H atoms are omitted for clarity. (f) Changes of the fluorescence intensity of HOF-20 aqueous suspensions upon addition of different analytes (10 μL, 100 mM). Reproduced from ref. 53. Copyright 2020 American Chemical Society.

acid)naphthalimide (H_4L) as a hydrogen bond building unit to construct a new type of HOFs, called FJU-200.[144] When immersed in an aniline solution, FJU-200 changed from its intrinsic light yellow to deep red. This is the first example of the double induction of color change and photoluminescence quenching in aniline detection. HOFs can also be used to detect other hazardous environmental pollutants and metal ions by the fluorescence attenuation method.[48,50]

3.3.2 Temperature sensing. A luminescent thermometer has high accuracy, short response time, and high spatial resolution, and also it can resist strong electric and magnetic fields and contactlessly detect the temperature of biological fluids and fast-moving objects.[145,146] Since 2012, among these luminescent materials, a series of unique solid thermometers of lanthanide MOF (Ln-MOF) mixed materials have been developed and widely used as a thermal probe for luminescent thermometers.[147–149]

As MOFs and HOFs exhibit similar porosity, a lanthanide-HOF can also be prepared by a specific method to study its performance as a luminescent thermometer. Cao and co-workers used a multi-step method to successfully prepare lanthanide-HOFs and test them as fluorescence sensors for proportional temperature sensing.[106] First, H_4TCBP was selected as a hydrogen bond building unit, and a porous and stable HOF was prepared by a simple solution method, denoted as HOF-TCBP. Second, through the post-modification with Eu^{2+}, a HOF with lanthanide function was obtained, named Eu@HOF-TCBP. Third, Eu@HOF-TCBP was further electrophoretically deposited on a zinc plate to prepare a thin film with high crystallinity and uniform texture (Fig. 19a). As expected, the prepared film exhibited dual emission peaks, one of which was from HOF-TCBP around 400 nm, and the other from Eu ions around 613 nm. The temperature-dependent PL spectrum showed that when the temperature gradually increased, the emission intensity of the Eu@HOF-TCBP film at 400 nm gradually decreased (Fig. 19b and c). In addition, when the temperature increased, the light-emitting color of the film changed significantly, proving that the temperature change could be observed with the naked eyes.

3.3.3 Electrochromic materials. Electrochromism describes the reversible color change of a material in response to external electronic stimuli. Electrochromic materials show reversible and stable color changes under external pressure and have broad application prospects in the fields of information storage, electronic displays, smart windows, dynamic mirrors, *etc.*[150]

In 2020, Cao and co-workers reported the first electrochromic HOF film.[107] The film exhibited uniform morphology, dense surface, high crystallinity, and reversible electrochromism. The transparent film was electrophoretically prepared at room temperature in only 2 min. As expected, the PFC-1 film deposited on FTO glass demonstrated reversible electrochromic properties, and its color gradually changed from yellow to blue-violet within the potential range of 0–1.6 V (Fig. 20a), and transmittance reduced from 75 to 25%. When a potential of 1–1.8 V was applied to the film, these peaks gradually decreased, while new peaks appeared and slowly moved around 600 and 560 nm (Fig. 20b). More interestingly, when reverse potentials of −0.5, −0.7, and −0.9 V were applied, the absorption intensity at 600 nm attenuated, while the absorbance near 400 and 450 nm returned to its original state, which fully validated the nano-PFC-1 reversible electrochromic behavior of the film (Fig. 20b). Therefore, the color-changing potential of HOFs indicated promising electrochromic applications. When the potential was switched between −0.9 and 1.5 V, the transmittance of the film changed from the original state to a colored state, and the contrast transmittance (50%) remained stable for 20 cycles (Fig. 20d and e). The reduction of the anode and the cathode peaks of the nano-PFC-1 thin film was

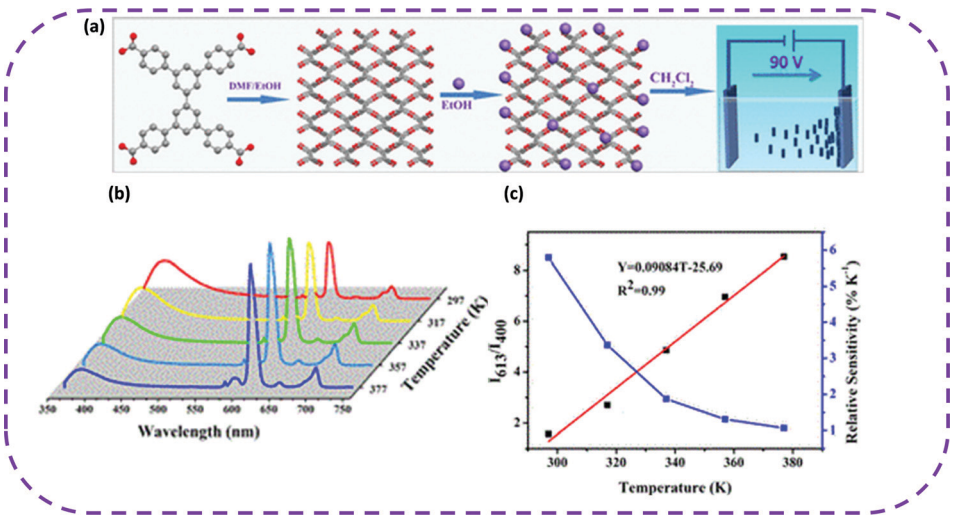

Fig. 19 (a) Preparation of Eu@HOF-TCBP and Eu@HOF-TCBP films *via* electrophoretic deposition at room temperature. Color code: O, red; C, gray; and Eu, purple. (b) Photoluminescence (PL) spectra of the Eu@HOF-TCBP film excited at 330 nm in the range of 297–377 K. (c) Relationship of the intensity ratio (*Y*) of 613 and 400 nm *versus* temperature and the relative sensitivity *versus* temperature. Inset: the equation fitting the curve of intensity ratio (*Y*) to temperature (*T*). Reproduced from ref. 106. Copyright 2020 American Chemical Society.

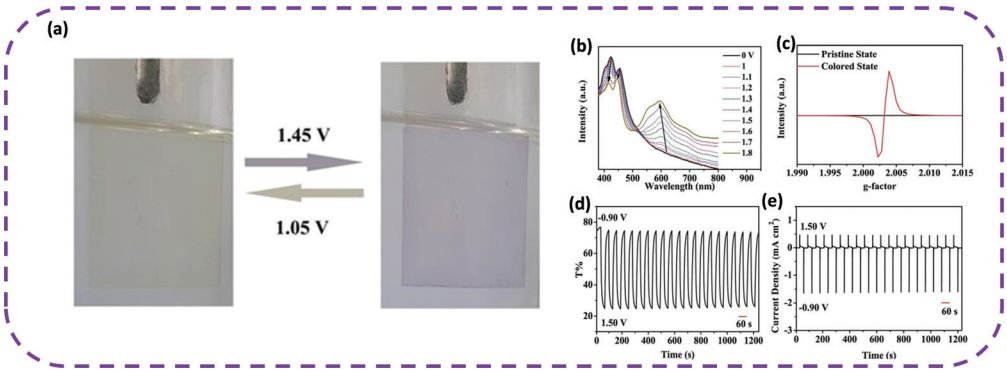

Fig. 20 (a) Photographs of a nano-PFC-1 EC film with applied potentials of 1.45 and 1.05 V during the CV scan (*vs.* Ag/AgCl). (b) UV-vis spectra of the nano-PFC-1 film at different potentials. (c) EPR spectra of nano-PFC-1 scraped from the substrate in the pristine state (0 V) and colored state (1.5 V). (d and e) Transmittance and current density changes of the nano-PFC-1 film observed at 600 nm for 20 cycles by switching the potential between −0.9 and +1.5 V. Reproduced from ref. 107. Copyright 2020 Wiley-VCH.

negligible after 500 CV cycles. After long-term scanning, no color change occurred on the film, indicating its ability to be reused. Due to the structural defects of nano-PFC-1 and the unbound carboxyl groups inevitably produced on the surface of the particles, the film was uniformly modified by Fe^{2+} ions as expected after being treated with $FeSO_4$ ethanol solution, named Fe@nano-PFC-1. The CV curve of Fe@nano-PFC-1 exhibited an additional reversible redox peak, which was completely different from the nano-PFC-1 film. Therefore, the obtained Fe@nano-PFC-1 film showed a continuous color change throughout the CV process. In summary, HOF materials can achieve tunable electrochromism *via* simple modification methods.

In summary, due to their unique advantages, HOFs were applied in the field of electrochromism. On the one hand, HOFs assemble with electrochromic parts by hydrogen bonding without introducing unnecessary components, which provides an economical and simple method of designing electrochromic materials. On the other hand, unique solution processability and easy regeneration of HOFs greatly facilitate the manufacturing process and reuse. In addition, facile modification, structural tunability, and high porosity further allow tuning of HOFs at the atomic level and accelerate electron transfer rates, thus improving electrochromic performance. Consequently, HOFs have great potential in the field of electrochromism.

3.3.4 Ultralong organic phosphorescent (UOP) materials. Cost efficiency and high biocompatibility of ultra-long organic phosphorescent (UOP) materials recommend them for potential applications in light technology, catalytic technology, biochemistry, and medical imaging.[151–153] However, there are still many problems to achieving an ultra-long luminescence lifetime of UOP materials, such as non-metal-induced spin–orbit coupling (SOC), low transmission efficiency between systems, the rapid non-radiative decay rate of triplet excitons, and unpredictable explosive killers (water and oxygen). Since the rigid crystal matrix can significantly reduce the proportion of non-radiative transitions,[154] HOFs, as the most representative crystalline organic materials, are considered the most promising candidate for UOP materials.

In 2018, Cai *et al.* designed a three-arm carbazole derivative PhTCz, and used the strong π–π interaction in the layer to build a hydrogen-bonded organic aromatic skeleton (termed as PhTCz-1, PhTCz-2, and PhTCz-3), which became the first example of metal-rare porous materials that achieved ultra-long phosphorescence at room temperature (Fig. 21a and b).[51] Like PhTCz-1, ultra-long yellow phosphorescence can be observed under environmental conditions (Fig. 21d). However, PhTCz-2 and PhTCz-3 did not exhibit UOP visible with the naked eye under the same environmental conditions (Fig. 21c and d). However, the ultra-long yellow phosphorescence of PhTCz-2 and PhTCz-3 was observed under an N_2 atmosphere. What's more attractive is that the UOP intensity of PhTCz-2 and PhTCz-3 crystals was closely related to oxygen concentration. This phenomenon fully proves the huge application potential of phosphorescent porous materials in oxygen sensing.

3.3.5 Micro-laser. Micro-lasers have received increasing attention because of their important roles in laser displays, on-chip optical communications, chemical sensing, and other fields.[155,156] Consequently, Zhao and co-workers first reported the application of HOFs in the field of micro-lasers.[102] A tetrastyrene chromophore with significant solid optical gain characteristics was selected as the main chain, and the cyano group was used as a hydrogen bond acceptor. Two kinds of microcrystals, HOF-FJU-4 and HOF-FJU-5, were formed by self-assembly in solution. The PL diagram showed that the two obtained crystallites exhibited regular shapes, with a smooth and flat surface. High-quality microcrystals with regular shapes provided efficient optical confinement.[157–159] Interestingly, HOF-FJU-4 and HOF-FJU-5 microcrystals exhibited distinct luminescence characteristics: strong blue (483 nm) and bright green (506 nm), respectively. Moreover, the high-quality microwires of HOF-FJU-4 and HOF-FJU-5 provided favorable conditions for constructing wavelength-tunable lasers. The laser spectral test, under the same size, indicated a laser threshold of HOF-FJU-4 microwire of about 545 nJ cm^{-2}, while the laser threshold of HOF-FJU-5 microwire was about 627 nJ cm^{-2}.

In conclusion, the first wavelength-tunable micro-laser was achieved using HOF microcrystals. We believe that this could

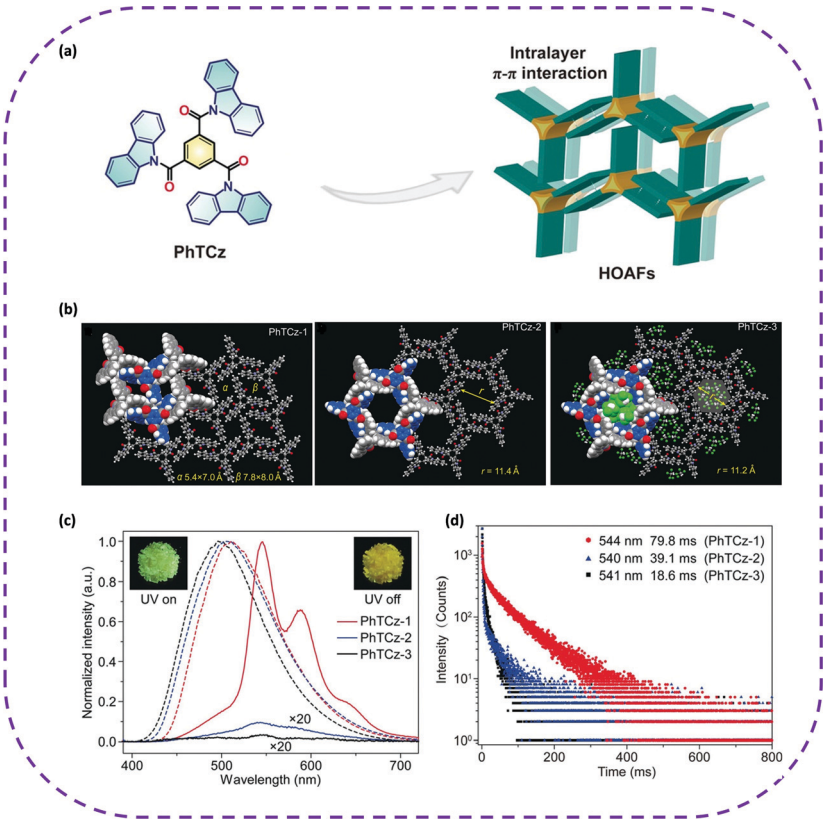

Fig. 21 (a) Hydrogen-bonded aromatic frameworks (HOAFs) based on PhTCz molecules. (b) Molecular stacking of three types of HOAFs of PhTCz-1, PhTCz-2 and PhTCz-3. (c) Steady-state photoluminescence (dashed lines) and phosphorescence spectra (solid lines) of PhTCz-1 (red), PhTCz-2 (blue), and PhTCz-3 (black) excited by a 365 nm light under ambient conditions. Phosphorescence signals of PhTCz-2 and PhTCz-3 were amplified (20×). Inset: Photographs of PhTCz-1 under a 365 nm UV light and after the UV light was switched off. (d) Lifetime decay profiles of PhTCz-1, PhTCz-2 and PhTCz-3 monitored at 544, 540 and 541 nm excited at 365 nm under ambient conditions, respectively. Reproduced from ref. 51. Copyright 2018 Wiley-VCH.

provide new insight into the future development of HOF nanophotonic devices with ideal laser characteristics. At the same time, new research directions and fields enrich HOF chemistry, thereby opening up new directions for providing diversified functions and applications.

3.4 Catalysts

3.4.1 Heterogeneous catalysis. Heterogeneous catalysis has always occupied an important position in the chemical industry.[160] Finding a new type of highly efficient and easy-to-recover heterogeneous catalyst has been in the research focus for a long time. So far, widely used heterogeneous catalysts have good activity, stability, and porosity, and they are mostly MOFs and COFs.[161,162] On the contrary, until recently, there were very few reports on HOF-based catalysts due to their relatively poor stability. The construction of HOF-based catalysts can be mainly achieved by the following methods. First, the catalyst is encapsulated in the pores of HOFs. Second, the catalytic units are used as constructing units for HOFs. Finally, by modifying the pore surface, more active sites are exposed on the pore wall.

In 2019, Han *et al.* reported a heterogeneous catalyst based on HOFs obtained through a metal-modified procedure, named HOF-19.[56] HOF-19 was constructed from amino-substituted cage-like building block, bis-(tetraoxacalix[2]arene[2]triazine) (L) (Fig. 22a). The synthesized HOF exhibited one-dimensional channels with a size of 8.0 × 13.6 Å (Fig. 22b). The activated HOF-19 was soaked in a palladium acetate and acetone solution to successfully prepare HOF-19⊃Pd(II) (Fig. 22d). The resulting complex could be used to catalyze the Suzuki–Miyaura coupling reaction (Fig. 22c). What's even more amazing is that HOF-19⊃Pd(II) maintained good catalytic activity and crystallinity after four reaction cycles in the 4-bromobenzonitrile conversion reaction. In addition, the catalyst could be regenerated by a simple recrystallization method, and the separation yield of 4-bromobenzonitrile was maintained by 92%. This work fully illustrates the huge application prospects of HOF materials in the field of heterogeneous catalysis.

3.4.2 Electrocatalysis. With the rapid development of industrialization, there is an urgent need for new alternative clean energy. Hydrogen power is recognized as the cleanest energy in the 21st century. Compared with other hydrogen production methods, hydrogen evolution from electrolysis water is a commonly used method with a good application prospect. However, the most effective catalyst for the electrochemical hydrogen production reaction (HER) is platinum, which increases the hydrogen production cost. Therefore, an electrocatalyst with high performance and low cost is urgently needed. So far, porous materials, such as COFs and

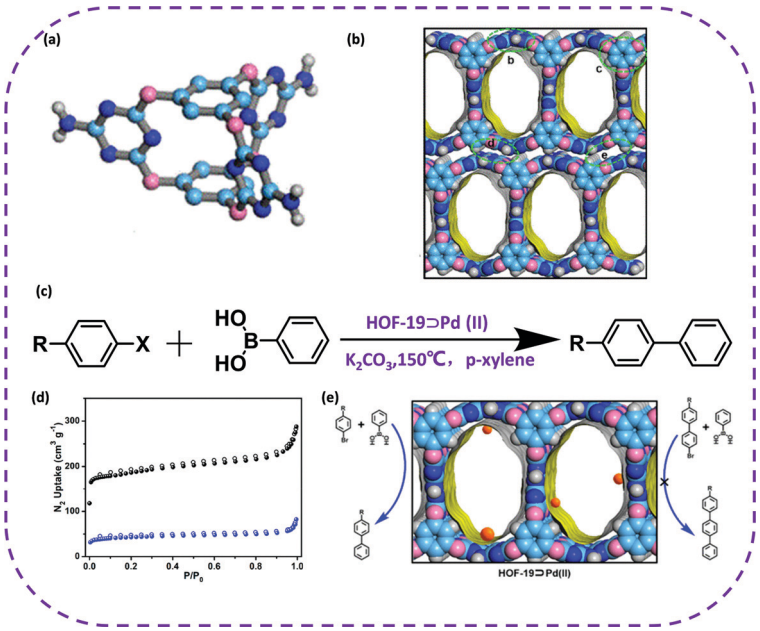

Fig. 22 (a) Organic building block of HOF-19. (b) A packing diagram of HOF-19 showing the 1D channel surfaces highlighted as yellow/gray (inner/outer) curved planes (C, slight cyan; O, pink; N, blue; and H, white). (c) The Suzuki–Miyaura coupling reaction that HOF-19⊃Pd(II) catalyze (R: –CHO, –CN, –H, $–NO_2$, –OMe; X: Br, I). (d) X-ray crystal structure of HOF-19⊃Pd(II). Reproduced from ref. 56. Copyright 2019 American Chemical Society.

conjugated triazine frameworks (CTFs), have been widely used as electrocatalysts.[163–166] As special porous materials, HOFs have a similar structure and properties to those of COFs. Although the stability of HOFs is poor, this deficiency does not hinder their development and application based on rigid HOFs reported before. Therefore, the topology of HOFs can also be precisely regulated to expose more electrocatalytic active sites.

In 2019, Liu *et al.* first proposed HOFs based on metal complexes for electrocatalytic water splitting.[57] First, cheap raw materials were selected to synthesize HOF materials, namely HOF-Co, through a step-by-step method (Fig. 23). Second, bimetallic HOFs were crystallized on nickel foam (NF) using the same method, denoted as HOF-Co_xFe_{1-x}. Interestingly, the bimetallic HOF-$Co_{0.5}Fe_{0.5}$ grown *in situ* on nickel foam can achieve excellent electrocatalytic hydrogen evolution performance. In addition, the hydrogen evolution performance of HOFs grown *in situ* on nickel foam was tested under alkaline conditions. It is worth noting that these HOFs also exhibited

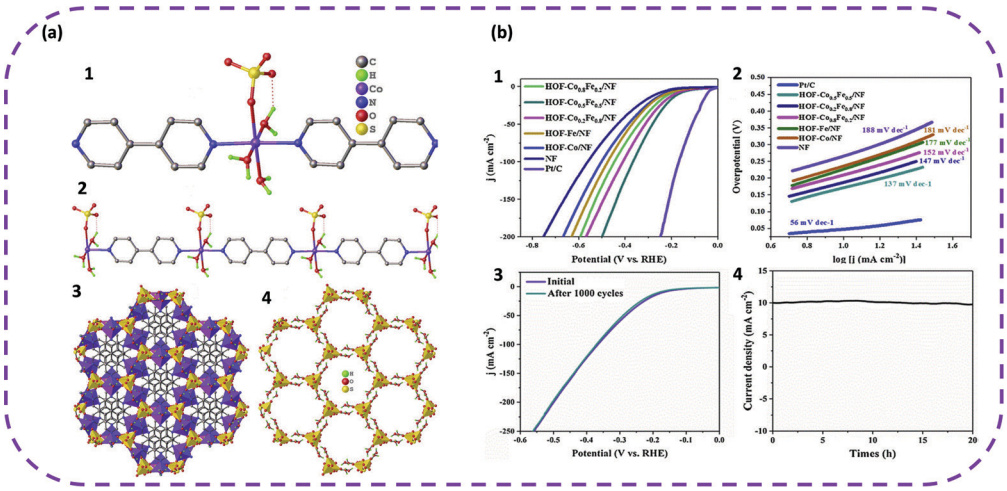

Fig. 23 (a) View of the structure of HOF-Co. (1) The coordination surrounding of metal ion. (2) The 1D metal complex connected by 4,4′-bpy ligand and containing abundant coordinated water molecules. (3) The 3D framework of HOF-Co. Metal and SO_4^{2-} ions give the octahedral and tetrahedral configuration, respectively. (4) The 3D hydrogen-bonded nanotube-based framework just built on SO_4^{2-} and coordinated water molecules. (b) Electrochemical performance. (1) Polarization curves and (2) the corresponding Tafel plots of different samples. (3) Polarization curves of HOF-$Co_{0.5}Fe_{0.5}$/NF before and after 1000 cycles of CV scan. (4) Chronoamperometric curve of HOF-$Co_{0.5}Fe_{0.5}$/NF at the overpotential of 170 mV. Reproduced from ref. 57. Copyright 2019 Elsevier.

superior HER activity, and the overpotential followed the sequence of HOF-$Co_{0.5}Fe_{0.5}$/NF (170 mV) > HOF-$Co_{0.2}Fe_{0.8}$/NF (188 mV) > HOF-$Co_{0.8}Fe_{0.2}$/NF (211 mV) > HOF Fe/NF (227 mV) > HOF-Co/NF (237 mV) (Fig. 24b). Correspondingly, the calculated Tafel slope of HOF-$Co_{0.5}Fe_{0.5}$/NF was also smaller than that of monometallic HOFs and other bimetallic HOFs (Fig. 23b). In addition, after cycling 1000 CV, the polarization curve of HOF-$Co_{0.5}Fe_{0.5}$/NF was measured again, and it was found that the curves basically overlapped completely, which once again verified the stability of HOF-$Co_{0.5}Fe_{0.5}$/NF. Therefore, this study provides new insight for the further use of HOFs in electrocatalytic water splitting.

Recently, it has been proven that HOFs enable a new breakthrough in electrocatalytic hydrogen evolution. In 2020, Coskun *et al.* reported a metal-free hydrogen-bonded polymer to simulate a noble metal electrocatalyst.[55] In this work, conductive polydopamine (PDA) was explored as an electrocatalyst, whose organic surface can provide a significant degree of catalytic activity by structural design and tuning the electrical conductivity. First, an *ab initio* calculation method was used to analyze different types of H-bonds in polydopamine (PDA) (Fig. 24a). The calculation of density functional theory proved that keto-indoleamine functional groups could be introduced multiple times into the PDA structure to improve HER selectivity (Fig. 24b and c). Based on this conclusion, the performance of electrocatalytic hydrogen evolution was studied. When the current density was 10 mA cm^{-2}, DHI-PDA (DHI, 5,6-dihydroxyindole) required a lower potential than standard PDA* (Fig. 24d). The comparison results of the Tafel slope showed that DHI-PDA (80 mV dec^{-1}) was lower than PDA* (110 mV dec^{-1}), which fully indicated that the electrocatalytic performance of DHI-PDA was better than that of PDA* (Fig. 24e). However, the electrocatalytic system needs more in-depth study, especially the change in the electrocatalytic performance originating from an increased concentration of the proton-active element DHI, which promotes the active catalytic site close to the noble metal. As far as the long-term stability of the acid electrolyte is concerned, this system has large loopholes, but it also broadens the platform for applying HOFs in electrocatalysis.

3.4.3 Photocatalysis. Photocatalysis combines multidisciplinary fields, and it has been explored for decades to promote

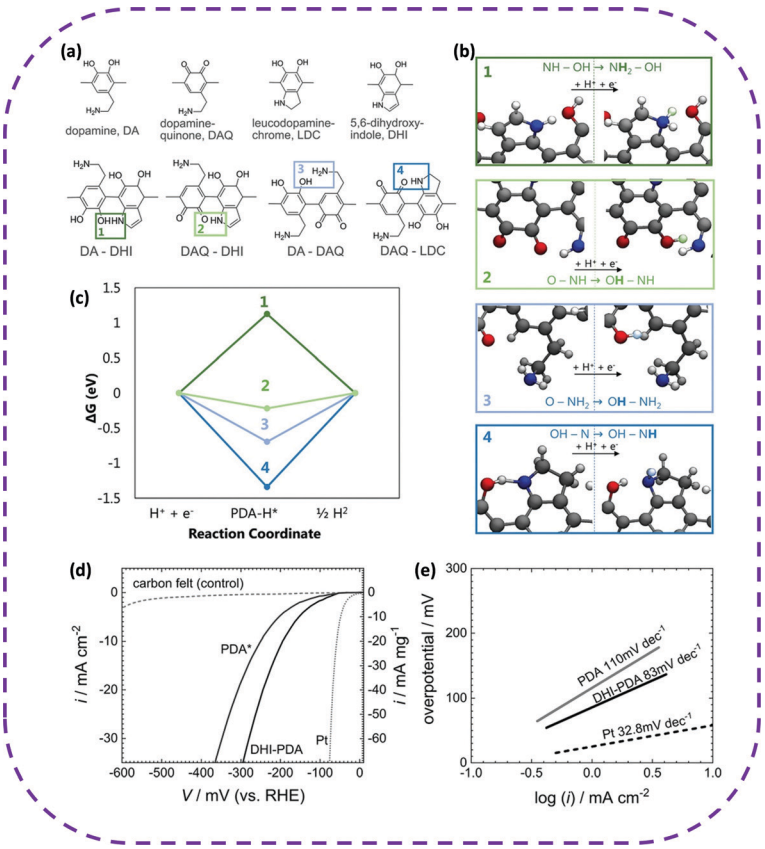

Fig. 24 DFT calculation of the hydrogen affinity of hydrogen bonding. (a) Monomer units in polydopamine (PDA) and illustration of the four dominant hydrogen-bonded motifs. (b) Simulation of Volmer reaction on hydroxyl-indoleamine (**1**, DA-DHI), keto-indoleamine (**2**, DAQ-DHI), hydroxyl-dopamine (**3**, DA-DAQ) and keto-indolineamine (**4**, DAQ-LDC). (c) Reaction energy diagrams for HER on the distinct motifs. The keto-indoleamine group (**2**, DAQ-DHI) offers the lowest energy for ΔGH* (−0.22 eV) while the other hydrogen-bonded motifs possess unfavorable energies for HER. Electrochemical characterization. (d) Voltammetric scans (10 mV s^{-1}, referred to active area and gravimetric) in 1 M TfOH electrolyte for HER showing the performance of PDA (standard) and DHI-PDA as compared to Pt (reference) and CF (blank control). (e) Tafel plot (log(*i*) *vs.* *η*) with the slopes indicated in the graph. The reference overpotential *η* (at 10 mA cm^{-2} planar current density) is 190 mV (DHI-PDA) and 270 mV (PDA). Reproduced from ref. 55. Copyright 2020 Wiley-VCH.

more efficient use of solar energy. Although photocatalysts have many shortcomings, such as low visible light utilization, high toxicity, and photocorrosion, which limit their further applications,[167] organic semiconductors with excellent properties have been extensively studied for photocatalysis due to their unique characteristics. Therefore, it is very important to develop an organic semiconductor that regulates its morphology. However, as a small branch of the organic semiconductor family, HOFs have huge application potential in photocatalysis.

Recently, Yu *et al.* have reported a new HOF synthesized by hydrogen-bonded guanin-quadruplex (Gquadruplex) directing the self-assembly of a 2,2′-bipyridine (bpy)-derived building block (L), named HOF-25.[168] HOF-25 was post-modified with $Re(CO)_5Cl$, and a porous HOF was obtained, $Re(bpy)(CO)_3Cl$, denoted as HOF-25-Re (Fig. 26a). Unexpectedly, it was found that HOF-25-Re was a stable and reusable heterogeneous catalyst due to the addition of the $[Ru(bpy)_3]Cl_2{\cdot}6H_2O$ photosensitizer to CH_3CN containing triisopropanolamine (TIPA). HOF-25-Re promoted the visible light reduction of carbon dioxide. The yield of CO in 3 cycles was relatively high, and CO selectivity reached 93% (Fig. 25a and b). HOF-25-Re photocatalyzing the conversion of CO_2 to CO could be maintained for 16 hours (8 cycles) before the catalyst was deactivated (Fig. 25c and d). Interestingly, after HOF-25-Re was inactivated, its photocatalytic performance could be restored by crystallization and post-modification. As photocatalysts, HOFs were preliminarily investigated in the aspects of photodegradation[169] and photocatalytic hydrogen evolution.[54] The above examples fully illustrate that HOFs are a unique choice for developing efficient and reusable photocatalysts.

3.5 Biological applications

The protection of biological components plays a vital role in the application of biotechnology.[170] It can increase the durability of enzymes in biocatalysis or the stability of biotherapeutics during the transportation and using process. A practical way to enhance the stability of enzymes is to encapsulate them in porous materials. Once enzymes are encapsulated in mesoporous silicon,[171] MOFs[172] and COFs,[173] they can avoid the influence of organic solvents and high temperatures to a certain extent. However, these porous host materials have some insurmountable disadvantages, such as poor biocompatibility, toxicity, and complex synthesis conditions. HOFs are metal-free, favoring superior biocompatibility and low toxicity, so they are among the best candidate materials for biological applications.

On the one hand, since HOFs have self-repairing properties, they are currently the most promising biomolecular packaging materials. In 2019, Liang *et al.* prepared a water-soluble stable HOF composed of tetraamide and tetracarboxylic acid, denoted as BioHOF-1.[58] In this work, two specific enzyme molecules (fluorescence-labeled catalase (FCAT) or fluorescence-labeled alcohol oxidase (FAO_X)) were selected to crystallize with BioHOF-1. Hence, two enzymes with immobilized complexes were constructed, named FCAT@BioHOF-1 and FAO_X@BioHOF-1 (Fig. 26a). It should be noted that the resulting enzyme complex exhibited high stability in water, phosphate buffer, and organic solvents. It maintained a relatively high activity, especially after heat treatment and trypsin and urea treatment (Fig. 26b and c). On the contrary, the free enzyme activity was rapidly lost under the same conditions, which fully illustrates that the BioHOF-1 coating significantly improved the stability of the encapsulated enzyme.

4. Prospects

As a new kind of porous crystalline material, HOFs are mainly self-assembled from organic molecules with light elements

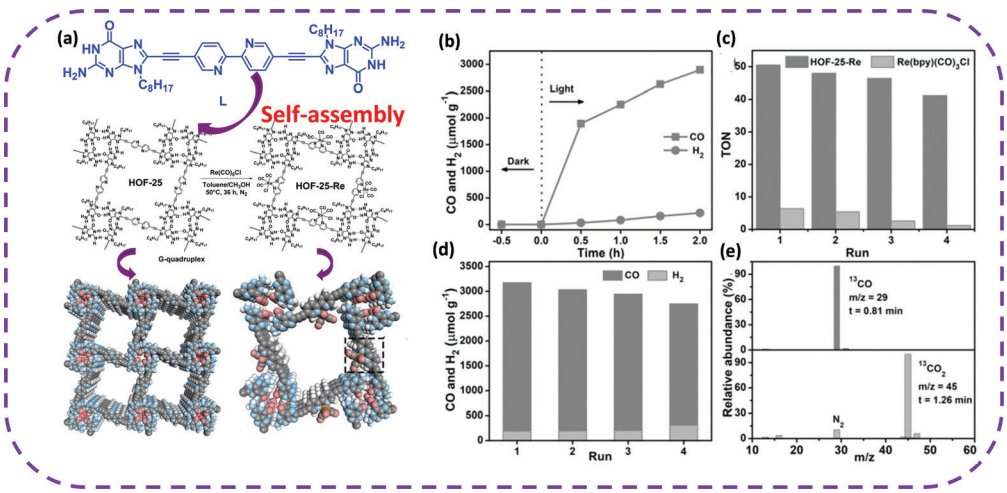

Fig. 25 (a) Self-assembly into HOF-25 and HOF-25Re crystal structure diagram. (b) Time-dependent CO and H_2 evolution for the visible-light irradiated photocatalytic system with HOF-25-Re and CO_2 at 1.0 bar in the presence of $[Ru(bpy)_3]Cl_2{\cdot}6H_2O$ and TIPA in CH_3CN. (c) The TON comparison of the CO_2 photoreduction between HOF-25-Re and $Re(bpy)(CO)_3Cl$ in heterogeneous and homogeneous phases, respectively. (d) Stability test of the HOF-25-Re photocatalyst with 2.0 h each run. (e) Mass spectrum of ^{13}CO produced from the photocatalytic reduction of $^{13}CO_2$. Reproduced from ref. 168. Copyright 2021 Wiley-VCH.

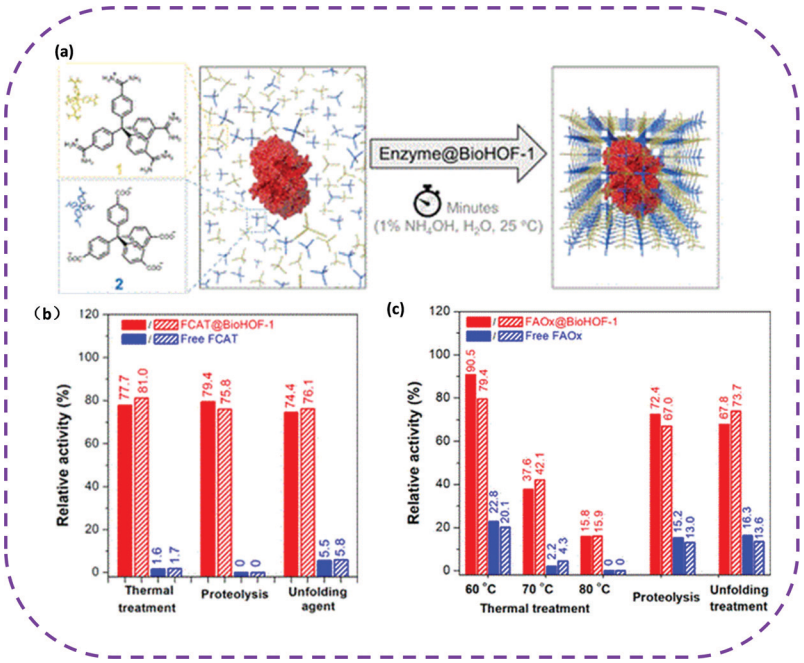

Fig. 26 (a) A schematic representation of the synthesis of enzyme@BioHOF-1 composite. (b) Relative activity (%) of free FCAT and FCAT@BioHOF-1 after thermal treatment (60 °C for 30 min), and exposure to trypsin (2 mg mL^{-1} for 2 h) and urea (6 M urea for 30 min). (c) Relative activity (%) of free FAOx and FAOx@BioHOF-1 after heating (60, 70, and 80 °C for 10 min) and exposure to trypsin (2 mg mL^{-1} for 2h) and urea (6 M urea for 30 min). Reproduced from ref. 58. Copyright 2019 American Chemical Society.

(C, H, O, N, B, *etc.*) through intermolecular interactions (hydrogen bonds, interactions, van der Waals forces, *etc.*). In this review, we highlighted the design principle about constructing HOFs with favorable stability and permanent porosity and summarized some major applications of HOFs. As mentioned above, HOFs have been designed, prepared, and applied in various fields based on the following characteristics. For example, (i) their flexible structure makes them the best candidates for assessing the fundamental structure of chiral molecules. (ii) HOFs constructed based on rigid molecules have high stability and can be used for gas separation, adsorption, and storage. (iii) HOFs constructed based on conjugated structures are good luminescent materials, which can be used for fluorescence sensing, fluorescence detection, and ultra-long phosphorescent materials. (iv) HOFs based on guanidine and sulfonate groups have excellent conductivity and can be used for proton conduction. (v) HOFs can also be applied in the field of catalysis by adjusting their structure and pore size to expose more active sites. (vi) HOFs without metal species have good biocompatibility and low toxicity, so biological applications have broad application prospects. (vii) Since pure organic compounds can be processed into various forms by simple methods, membrane-based HOFs have also been widely used in gas separation, temperature sensing, and luminescent materials. In summary, HOF materials may find pivotal roles in many fields in the future.

Compared with other interactions, hydrogen bonding in HOFs is weaker and conformationally more flexible, and it is difficult for HOFs to maintain their porous framework after removing solvent molecules, which hinders the development of HOFs. However, since Chen's group first reported the permanent pore microporous HOFs in 2011, HOFs have been developed rapidly, especially in recent years. A substantial breakthrough has been made in terms of porosity, which is even comparable to some extraordinary porous MOFs. Some HOFs can still retain the framework integrity under external stimuli, even better than most MOFs. More interestingly, self-repair of HOFs can be achieved through a simple solution treatment. With the continuous research on HOFs, huge enhancement in many fields might be expected.

However, HOFs still face several challenges, and future effort should be mainly focused on two aspects: molecular design and applications. For molecular design, we need more feasible and practical strategies to construct HOFs with a large surface area and high stability. In this issue, several factors need to be considered.

(i) Rigidity of the main chain structure

The stronger the molecular rigidity, the more difficult it is to change the direction of the molecular chain. This also fully shows that when selecting molecules, one should choose molecules with more benzene rings.

(ii) Strength and number of hydrogen bond sites

The sulfonic acid and the guanidine group are assisted by the charge between the cation and anion to form a hydrogen bond. DAT and its derivatives, which can serve as hydrogen bond acceptors or hydrogen bond donors, enable the formation of multiple N–H·bonds. Hence, these two types of molecules are also a good choice.

(iii) Interaction between building units and guest molecules

For example: introducing strong binding sites such as metal sites or Lewis acid/base sites into the pores of HOFs *via* pre-design or post-synthesis methods. In other words, in the early stage of molecular design, factors, such as the rigidity of the main chain structure, strength and number of hydrogen bond sites, the extension direction of hydrogen bonds, and interaction between structural units and guest molecules, should be considered, thus laying a foundation for the synthesis of highly stable HOFs.

HOFs have been applied in different fields, such as hydrocarbon separation, gas adsorption, proton conduction, sensing and fluorescence detection, catalysis, and biomedicine. Exploring new applications of HOFs is also the current challenge. The pores of HOFs are created by removing solvent from solvated crystals. This also shows that HOFs with channel restriction can minimize severe aggregation-caused quenching (ACQ) and twisted intramolecular charge transfer (TICT) loss of laser dyes by intramolecular rotation and weakening of intermolecular interactions; The smooth and flat morphology of HOFs can be used as a natural, high-quality resonant cavity. This manifests once again the great potential of HOFs in building highly stable, high-performance, low-threshold micro-lasers; The reversibility of hydrogen bonds can self-repair crystal defects to improve the framework order. An ordered framework is necessary for electron transmission. Logically, HOFs can also be used for flexible devices. Nevertheless, up to now, there are almost no reports on micro-lasers and flexible devices. Therefore, in the future, efforts should be made to pave the way toward applying HOFs in optoelectronics.

To sum up, after a decade of intensive research, the field of HOF materials is moving toward another powerful platform for developing multifunctional materials. With the continuous development of building units, HOF structures are enriched, and multifunctional HOFs are gradually realized. In short, HOFs can build more interesting and attractive multifunctional material platforms.

Author contributions

Lifang Chen: conceptualization, data curation, and writing-original draft preparation. Boying Zhang and Liling Chen: methodology and writing-original draft preparation. Haining Liu: writing-reviewing and Editing. Shanlin Qiao and Yongqi Hu: supervision.

Conflicts of interest

The authors declare that they have no conflict of interest.

Acknowledgements

We are grateful to the National Natural Science Foundation of China (Grant No. 22105058, 21805068) and Hebei (China) Natural Science Foundation for Youth (Grant No. B2021208073).

References

1 M. E. Davis, *Nature*, 2002, **417**, 813–821.
2 L. Tan and B. Tan, *Chem. Soc. Rev.*, 2017, **46**, 3322–3356.
3 H. Lyu, C. S. Diercks, C. Zhu and O. M. Yaghi, *J. Am. Chem. Soc.*, 2019, **141**, 6848–6852.
4 B. M. Weckhuysen and J. Yu, *Chem. Soc. Rev.*, 2015, **44**, 7022–7024.
5 M. Carreon, *J. Am. Chem. Soc.*, 2008, **130**, 13184.
6 J. Yu and R. Xu, *Acc. Chem. Res.*, 2010, **43**, 1195–1204.
7 J. Li, A. Corma and J. Yu, *Chem. Soc. Rev.*, 2015, **44**, 7112–7127.
8 M. Mon, X. Qu, J. Ferrando-Soria, I. Pellicer-Carreño, A. Sepúlveda-Escribano, E. V. Ramos-Fernandez, J. C. Jansen, D. Armentano and E. Pardo, *J. Mater. Chem. A*, 2017, **5**, 20120–20125.
9 Z. Bao, G. Chang, H. Xing, R. Krishna, Q. Ren and B. Chen, *Energy Environ. Sci.*, 2016, **9**, 3612–3641.
10 K. Jayaramulu, F. Geyer, A. Schneemann, Š. Kment, M. Otyepka, R. Zboril, D. Vollmer and R. A. Fischer, *Adv. Mater.*, 2019, **31**, 1970230.
11 A. E. Thorarinsdottir and T. D. Harris, *Chem. Rev.*, 2020, **120**, 8716–8789.
12 R. Gaillac, P. Pullumbi, K. A. Beyer, K. W. Chapman, D. A. Keen, T. D. Bennett and F.-X. Coudert, *Nat. Mater.*, 2017, **16**, 1149–1154.
13 S. Yuan, L. Feng, K. Wang, J. Pang, M. Bosch, C. Lollar, Y. Sun, J. Qin, X. Yang, P. Zhang, Q. Wang, L. Zou, Y. Zhang, L. Zhang, Y. Fang, J. Li and H.-C. Zhou, *Adv. Mater.*, 2018, **30**, 1870277.
14 Y. Cui, B. Li, H. He, W. Zhou, B. Chen and G. Qian, *Acc. Chem. Res.*, 2016, **49**, 483–493.
15 A. P. Côté, A. I. Benin, N. W. Ockwig, M. Keeffe, A. J. Matzger and O. M. Yaghi, *Science*, 2005, **310**, 1166.
16 P. J. Waller, F. Gándara and O. M. Yaghi, *Acc. Chem. Res.*, 2015, **48**, 3053–3063.
17 K. Geng, T. He, R. Liu, S. Dalapati, K. T. Tan, Z. Li, S. Tao, Y. Gong, Q. Jiang and D. Jiang, *Chem. Rev.*, 2020, **120**, 8814–8933.
18 Y. Li, W. Chen, G. Xing, D. Jiang and L. Chen, *Chem. Soc. Rev.*, 2020, **49**, 2852–2868.
19 J. Zhang, X. Han, X. Wu, Y. Liu and Y. Cui, *J. Am. Chem. Soc.*, 2017, **139**, 8277–8285.
20 M. S. Lohse and T. Bein, *Adv. Funct. Mater.*, 2018, **28**, 1870229.
21 Z. Wang, S. Zhang, Y. Chen, Z. Zhang and S. Ma, *Chem. Soc. Rev.*, 2020, **49**, 708–735.
22 S. Yuan, X. Li, J. Zhu, G. Zhang, P. Van Puyvelde and B. Van der Bruggen, *Chem. Soc. Rev.*, 2019, **48**, 2665–2681.
23 Z.-C. Guo, Z.-Q. Shi, X.-Y. Wang, Z.-F. Li and G. Li, *Coord. Chem. Rev.*, 2020, **422**, 213465.
24 H. Xu, S. Tao and D. Jiang, *Nat. Mater.*, 2016, **15**, 722–726.

25 Q. Yang, M. Luo, K. Liu, H. Cao and H. Yan, *Appl. Catal., B*, 2020, **276**, 119174.
26 T. Banerjee, K. Gottschling, G. Savasci, C. Ochsenfeld and B. V. Lotsch, *ACS Energy Lett.*, 2018, **3**, 400–409.
27 J. R. Holst, A. Trewin and A. I. Cooper, *Nat. Chem.*, 2010, **2**, 915–920.
28 M. A. Little and A. I. Cooper, *Adv. Funct. Mater.*, 2020, **30**, 1909842.
29 A. I. Cooper, *ACS Cent. Sci.*, 2017, **3**, 544–553.
30 C. G. Bezzu, L. A. Burt, C. J. McMonagle, S. A. Moggach, B. M. Kariuki, D. R. Allan, M. Warren and N. B. McKeown, *Nat. Mater.*, 2019, **18**, 740–745.
31 B. Kohl, F. Rominger and M. Mastalerz, *Chem. – Eur. J.*, 2015, **21**, 17308–17313.
32 Y.-T. Wang, C. McHale, X. Wang, C.-K. Chang, Y.-C. Chuang, W. Kaveevivitchai, O. Š. Miljanić and T.-H. Chen, *Angew. Chem., Int. Ed.*, 2021, **60**, 14717.
33 M. Kimura, M. Yoshida, S. Fujii, A. Miura, K. Ueno, Y. Shigeta, A. Kobayashi and M. Kato, *Chem. Commun.*, 2020, **56**, 12989–12992.
34 R.-B. Lin, Y. He, P. Li, H. Wang, W. Zhou and B. Chen, *Chem. Soc. Rev.*, 2019, **48**, 1362–1389.
35 I. Hisaki, C. Xin, K. Takahashi and T. Nakamura, *Angew. Chem., Int. Ed.*, 2019, **58**, 11160–11170.
36 B. Wang, R.-B. Lin, Z. Zhang, S. Xiang and B. Chen, *J. Am. Chem. Soc.*, 2020, **142**, 14399–14416.
37 W. Yang, A. Greenaway, X. Lin, R. Matsuda, A. J. Blake, C. Wilson, W. Lewis, P. Hubberstey, S. Kitagawa, N. R. Champness and M. Schröder, *J. Am. Chem. Soc.*, 2010, **132**, 14457–14469.
38 S. Yu, G.-L. Xing, L.-H. Chen, T. Ben and B.-L. Su, *Adv. Mater.*, 2020, **32**, 2003270.
39 T.-U. Yoon, S. B. Baek, D. Kim, E.-J. Kim, W.-G. Lee, B. K. Singh, M. S. Lah, Y.-S. Bae and K. S. Kim, *Chem. Commun.*, 2018, **54**, 9360–9363.
40 Q. Yin, Y.-L. Li, L. Li, J. Lü, T.-F. Liu and R. Cao, *ACS Appl. Mater. Interfaces*, 2019, **11**, 17823–17827.
41 X. Zhang, L. Li, J.-X. Wang, H.-M. Wen, R. Krishna, H. Wu, W. Zhou, Z.-N. Chen, B. Li, G. Qian and B. Chen, *J. Am. Chem. Soc.*, 2020, **142**, 633–640.
42 P. Li, Y. He, H. D. Arman, R. Krishna, H. Wang, L. Weng and B. Chen, *Chem. Commun.*, 2014, **50**, 13081–13084.
43 J. Liang, S. Xing, P. Brandt, A. Nuhnen, C. Schlüsener, Y. Sun and C. Janiak, *J. Mater. Chem. A*, 2020, **8**, 19799–19804.
44 S. Nandi, D. Chakraborty and R. Vaidhyanathan, *Chem. Commun.*, 2016, **52**, 7249–7252.
45 H. Wang, B. Li, H. Wu, T.-L. Hu, Z. Yao, W. Zhou, S. Xiang and B. Chen, *J. Am. Chem. Soc.*, 2015, **137**, 9963–9970.
46 A. Karmakar, R. Illathvalappil, B. Anothumakkool, A. Sen, P. Samanta, A. V. Desai, S. Kurungot and S. K. Ghosh, *Angew. Chem., Int. Ed.*, 2016, **55**, 10667–10671.
47 Y. Wang, M. Zhang, Q. Yang, J. Yin, D. Liu, Y. Shang, Z. Kang, R. Wang, D. Sun and J. Jiang, *Chem. Commun.*, 2020, **56**, 15529–15532.
48 Z. Sun, Y. Li, L. Chen, X. Jing and Z. Xie, *Cryst. Growth Des.*, 2015, **15**, 542–545.
49 H. Zhou, Q. Ye, X. Wu, J. Song, C. M. Cho, Y. Zong, B. Z. Tang, T. S. A. Hor, E. K. L. Yeow and J. Xu, *J. Mater. Chem. C*, 2015, **3**, 11874–11880.
50 H. Wang, Z. Bao, H. Wu, R.-B. Lin, W. Zhou, T.-L. Hu, B. Li, J. C.-G. Zhao and B. Chen, *Chem. Commun.*, 2017, **53**, 11150–11153.
51 S. Cai, H. Shi, Z. Zhang, X. Wang, H. Ma, N. Gan, Q. Wu, Z. Cheng, K. Ling, M. Gu, C. Ma, L. Gu, Z. An and W. Huang, *Angew. Chem., Int. Ed.*, 2018, **57**, 4005–4009.
52 Y. Wang, D. Liu, J. Yin, Y. Shang, J. Du, Z. Kang, R. Wang, Y. Chen, D. Sun and J. Jiang, *Chem. Commun.*, 2020, **56**, 703–706.
53 B. Wang, R. He, L.-H. Xie, Z.-J. Lin, X. Zhang, J. Wang, H. Huang, Z. Zhang, K. S. Schanze, J. Zhang, S. Xiang and B. Chen, *J. Am. Chem. Soc.*, 2020, **142**, 12478–12485.
54 Y. Tang, M. Yuan, B. Jiang, Y. Xiao, Y. Fu, S. Chen, Z. Deng, Q. Pan, C. Tian and H. Fu, *J. Mater. Chem. A*, 2017, **5**, 21979–21985.
55 H. Coskun, A. Aljabour, P. de Luna, H. Sun, N. Nishiumi, T. Yoshida, G. Koller, M. G. Ramsey, T. Greunz, D. Stifter, M. Strobel, S. Hild, A. W. Hassel, N. S. Sariciftci, E. H. Sargent and P. Stadler, *Adv. Mater.*, 2020, **32**, 1902177.
56 B. Han, H. Wang, C. Wang, H. Wu, W. Zhou, B. Chen and J. Jiang, *J. Am. Chem. Soc.*, 2019, **141**, 8737–8740.
57 F. Q. Liu, J. W. Liu, Z. Gao, L. Wang, X.-Z. Fu, L. X. Yang, Y. Tao, W. H. Yin and F. Luo, *Appl. Catal., B*, 2019, **258**, 117973.
58 W. Liang, F. Carraro, M. B. Solomon, S. G. Bell, H. Amenitsch, C. J. Sumby, N. G. White, P. Falcaro and C. J. Doonan, *J. Am. Chem. Soc.*, 2019, **141**, 14298–14305.
59 J. Bernstein, R. E. Davis, L. Shimoni and N.-L. Chang, *Angew. Chem., Int. Ed. Engl.*, 1995, **34**, 1555–1573.
60 I. Hisaki, S. Nakagawa, N. Ikenaka, Y. Imamura, M. Katouda, M. Tashiro, H. Tsuchida, T. Ogoshi, H. Sato, N. Tohnai and M. Miyata, *J. Am. Chem. Soc.*, 2016, **138**, 6617–6628.
61 O. Ivasenko and D. F. Perepichka, *Chem. Soc. Rev.*, 2011, **40**, 191–206.
62 T.-H. Chen, I. Popov, W. Kaveevivitchai, Y.-C. Chuang, Y.-S. Chen, O. Daugulis, A. J. Jacobson and O. Š. Miljanić, *Nat. Commun.*, 2014, **5**, 5131.
63 K. D. M. Harris, *Chem. Soc. Rev.*, 1997, **26**, 279–289.
64 J. Yang, M. B. Dewal, S. Profeta, M. D. Smith, Y. Li and L. S. Shimizu, *J. Am. Chem. Soc.*, 2008, **130**, 612–621.
65 J. Yang, J. Wang, B. Hou, X. Huang, T. Wang, Y. Bao and H. Hao, *Chem. Eng. J.*, 2020, **399**, 125873.
66 P. Li, Y. He, Y. Zhao, L. Weng, H. Wang, R. Krishna, H. Wu, W. Zhou, M. O'Keeffe, Y. Han and B. Chen, *Angew. Chem., Int. Ed.*, 2015, **54**, 574–577.
67 J. Nicks, S. A. Boer, N. G. White and J. A. Foster, *Chem. Sci.*, 2021, **12**, 3322–3327.
68 M. Mastalerz and I. M. Oppel, *Angew. Chem., Int. Ed.*, 2012, **51**, 5252–5255.
69 M. I. Hashim, H. T. M. Le, T.-H. Chen, Y.-S. Chen, O. Daugulis, C.-W. Hsu, A. J. Jacobson, W. Kaveevivitchai, X. Liang, T. Makarenko, O. Š. Miljanić, I. Popovs,

H. V. Tran, X. Wang, C.-H. Wu and J. I. Wu, *J. Am. Chem. Soc.*, 2018, **140**, 6014–6026.
70 J.-X. Wang, X.-W. Gu, Y.-X. Lin, B. Li and G. Qian, *ACS Mater. Lett.*, 2021, **3**, 497–503.
71 K. Ma, P. Li, J. H. Xin, Y. Chen, Z. Chen, S. Goswami, X. Liu, S. Kato, H. Chen, X. Zhang, J. Bai, M. C. Wasson, R. R. Maldonado, R. Q. Snurr and O. K. Farha, *Cell Rep. Phys. Sci.*, 2020, **1**, 100024.
72 W. Yang, J. Wang, H. Wang, Z. Bao, J. C.-G. Zhao and B. Chen, *Cryst. Growth Des.*, 2017, **17**, 6132–6137.
73 P. Li, Y. He, J. Guang, L. Weng, J. C.-G. Zhao, S. Xiang and B. Chen, *J. Am. Chem. Soc.*, 2014, **136**, 547–549.
74 Y.-L. Li, E. V. Alexandrov, Q. Yin, L. Li, Z.-B. Fang, W. Yuan, D. M. Proserpio and T.-F. Liu, *J. Am. Chem. Soc.*, 2020, **142**, 7218–7224.
75 P. Li, P. Li, M. R. Ryder, Z. Liu, C. L. Stern, O. K. Farha and J. F. Stoddart, *Angew. Chem., Int. Ed.*, 2019, **58**, 1664–1669.
76 J. T. A. Jones, T. Hasell, X. Wu, J. Bacsa, K. E. Jelfs, M. Schmidtmann, S. Y. Chong, D. J. Adams, A. Trewin, F. Schiffman, F. Cora, B. Slater, A. Steiner, G. M. Day and A. I. Cooper, *Nature*, 2011, **474**, 367–371.
77 A. Pulido, L. Chen, T. Kaczorowski, D. Holden, M. A. Little, S. Y. Chong, B. J. Slater, D. P. McMahon, B. Bonillo, C. J. Stackhouse, A. Stephenson, C. M. Kane, R. Clowes, T. Hasell, A. I. Cooper and G. M. Day, *Nature*, 2017, **543**, 657–664.
78 C. Zhao, L. Chen, Y. Che, Z. Pang, X. Wu, Y. Lu, H. Liu, G. M. Day and A. I. Cooper, *Nat. Commun.*, 2021, **12**, 817.
79 J. A. Zerkowski, J. C. MacDonald and G. M. Whitesides, *Chem. Mater.*, 1994, **6**, 1250–1257.
80 F. H. Beijer, R. P. Sijbesma, J. A. J. M. Vekemans, E. W. Meijer, H. Kooijman and A. L. Spek, *J. Org. Chem.*, 1996, **61**, 6371–6380.
81 P. Brunet, M. Simard and J. D. Wuest, *J. Am. Chem. Soc.*, 1997, **119**, 2737–2738.
82 Y. He, S. Xiang and B. Chen, *J. Am. Chem. Soc.*, 2011, **133**, 14570–14573.
83 W. Yang, F. Yang, T.-L. Hu, S. C. King, H. Wang, H. Wu, W. Zhou, J.-R. Li, H. D. Arman and B. Chen, *Cryst. Growth Des.*, 2016, **16**, 5831–5835.
84 W. Yang, B. Li, H. Wang, O. Alduhaish, K. Alfooty, M. A. Zayed, P. Li, H. D. Arman and B. Chen, *Cryst. Growth Des.*, 2015, **15**, 2000–2004.
85 H. Wang, H. Wu, J. Kan, G. Chang, Z. Yao, B. Li, W. Zhou, S. Xiang, J. Cong-Gui Zhao and B. Chen, *J. Mater. Chem. A*, 2017, **5**, 8292–8296.
86 S. Feng, Y. Shang, Z. Wang, Z. Kang, R. Wang, J. Jiang, L. Fan, W. Fan, Z. Liu, G. Kong, Y. Feng, S. Hu, H. Guo and D. Sun, *Angew. Chem., Int. Ed.*, 2020, **59**, 3840–3845.
87 C. A. Zentner, H. W. H. Lai, J. T. Greenfield, R. A. Wiscons, M. Zeller, C. F. Campana, O. Talu, S. A. FitzGerald and J. L. C. Rowsell, *Chem. Commun.*, 2015, **51**, 11642–11645.
88 I. Hisaki, N. Ikenaka, E. Gomez, B. Cohen, N. Tohnai and A. Douhal, *Chem. – Eur. J.*, 2017, **23**, 11611–11619.
89 F. Hu, C. Liu, M. Wu, J. Pang, F. Jiang, D. Yuan and M. Hong, *Angew. Chem., Int. Ed.*, 2017, **56**, 2101–2104.
90 Q. Yin, P. Zhao, R.-J. Sa, G.-C. Chen, J. Lü, T.-F. Liu and R. Cao, *Angew. Chem., Int. Ed.*, 2018, **57**, 7691–7696.
91 I. Hisaki, Y. Suzuki, E. Gomez, B. Cohen, N. Tohnai and A. Douhal, *Angew. Chem., Int. Ed.*, 2018, **57**, 12650–12655.
92 W. Yang, W. Zhou and B. Chen, *Cryst. Growth Des.*, 2019, **19**, 5184–5188.
93 P. Cui, E. Svensson Grape, P. R. Spackman, Y. Wu, R. Clowes, G. M. Day, A. K. Inge, M. A. Little and A. I. Cooper, *J. Am. Chem. Soc.*, 2020, **142**, 12743–12750.
94 Y. Suzuki, N. Tohnai, A. Saeki and I. Hisaki, *Chem. Commun.*, 2020, **56**, 13369–13372.
95 E. Gomez, M. R. di Nunzio, M. Moreno, I. Hisaki and A. Douhal, *J. Phys. Chem. C*, 2020, **124**, 6938–6951.
96 M. D. Ward, *Chem. Commun.*, 2005, 5838–5842, DOI: 10.1039/B513077H.
97 V. A. Russell, M. C. Etter and M. D. Ward, *J. Am. Chem. Soc.*, 1994, **116**, 1941–1952.
98 V. A. Russell, M. C. Etter and M. D. Ward, *Chem. Mater.*, 1994, **6**, 1206–1217.
99 Y. Liu, W. Xiao, J. J. Yi, C. Hu, S.-J. Park and M. D. Ward, *J. Am. Chem. Soc.*, 2015, **137**, 3386–3392.
100 D. W. Kang, M. Kang, H. Kim, J. H. Choe, D. W. Kim, J. R. Park, W. R. Lee, D. Moon and C. S. Hong, *Angew. Chem., Int. Ed.*, 2019, **58**, 16152–16155.
101 T. Yu, D. Ou, Z. Yang, Q. Huang, Z. Mao, J. Chen, Y. Zhang, S. Liu, J. Xu, M. R. Bryce and Z. Chi, *Chem. Sci.*, 2017, **8**, 1163–1168.
102 Y. Lv, D. Li, A. Ren, Z. Xiong, Y. Yao, K. Cai, S. Xiang, Z. Zhang and Y. S. Zhao, *ACS Appl. Mater. Interfaces*, 2021, **13**, 28662–28667.
103 E. Arunan, G. R. Desiraju, R. A. Klein, J. Sadlej, S. Scheiner, I. Alkorta, D. C. Clary, R. H. Crabtree, J. J. Dannenberg, P. Hobza, H. G. Kjaergaard, A. C. Legon, B. Mennucci and D. J. Nesbitt, *Pure Appl. Chem.*, 2011, **83**, 1637–1641.
104 Y. Yang, L. Li, R.-B. Lin, Y. Ye, Z. Yao, L. Yang, F. Xiang, S. Chen, Z. Zhang, S. Xiang and B. Chen, *Nat. Chem.*, 2021, **13**, 933–939.
105 Y.-H. Luo, L. Zhang, W.-X. Fang, S.-H. Ma, H. Dong, S. Su, Z.-Y. Zheng, D.-N. Li and L.-H. Zhai, *Chem. Commun.*, 2021, **57**, 5901–5904.
106 J.-f. Feng, X.-Y. Yan, Z.-Y. Ji, T.-F. Liu and R. Cao, *ACS Appl. Mater. Interfaces*, 2020, **12**, 29854–29860.
107 J.-f. Feng, T.-F. Liu and R. Cao, *Angew. Chem., Int. Ed.*, 2020, **59**, 22392–22396.
108 B.-T. Liu, X.-H. Pan, D.-Y. Nie, X.-J. Hu, E.-P. Liu and T.-F. Liu, *Adv. Mater.*, 2020, **32**, 2005912.
109 L. Liu, A. V. Puga, J. Cored, P. Concepción, V. Pérez-Dieste, H. García and A. Corma, *Appl. Catal., B*, 2018, **235**, 186–196.
110 T. Ren, M. Patel and K. Blok, *Energy*, 2006, **31**, 425–451.
111 X. Wei, Z. Yin, K. Lyu, Z. Li, J. Gong, G. Wang, L. Xiao, J. Lu and L. Zhuang, *ACS Catal.*, 2020, **10**, 4103–4111.
112 Y.-Z. Li, G.-D. Wang, L.-N. Ma, L. Hou, Y.-Y. Wang and Z. Zhu, *ACS Appl. Mater. Interfaces*, 2021, **13**, 4102–4109.
113 H. Wang, Y. Liu and J. Li, *Adv. Mater.*, 2020, **32**, 2002603.

114 J. Wang, R. Krishna, T. Yang and S. Deng, *J. Mater. Chem. A*, 2016, **4**, 13957–13966.
115 Y. Wang, S. B. Peh and D. Zhao, *Small*, 2019, **15**, 1900058.
116 X. Zhang, J.-X. Wang, L. Li, J. Pei, R. Krishna, H. Wu, W. Zhou, G. Qian, B. Chen and B. Li, *Angew. Chem., Int. Ed.*, 2021, **60**, 10304–10310.
117 A. Baird and J. A. Maynard, *Science*, 2008, **320**, 315.
118 Q. Wang, J. Luo, Z. Zhong and A. Borgna, *Energy Environ. Sci.*, 2011, **4**, 42–55.
119 J. Cha, Y. S. Jo, H. Jeong, J. Han, S. W. Nam, K. H. Song and C. W. Yoon, *Appl. Energy*, 2018, **224**, 194–204.
120 M. C. Bryan, P. J. Dunn, D. Entwistle, F. Gallou, S. G. Koenig, J. D. Hayler, M. R. Hickey, S. Hughes, M. E. Kopach, G. Moine, P. Richardson, F. Roschangar, A. Steven and F. J. Weiberth, *Green Chem.*, 2018, **20**, 5082–5103.
121 A. J. Rieth and M. Dincă, *J. Am. Chem. Soc.*, 2018, **140**, 3461–3466.
122 J. F. Van Humbeck, T. M. McDonald, X. Jing, B. M. Wiers, G. Zhu and J. R. Long, *J. Am. Chem. Soc.*, 2014, **136**, 2432–2440.
123 C. J. Doonan, D. J. Tranchemontagne, T. G. Glover, J. R. Hunt and O. M. Yaghi, *Nat. Chem.*, 2010, **2**, 235–238.
124 D. W. Kang, M. Kang, M. Moon, H. Kim, S. Eom, J. H. Choe, W. R. Lee and C. S. Hong, *Chem. Sci.*, 2018, **9**, 6871–6877.
125 A. J. Rieth, Y. Tulchinsky and M. Dincă, *J. Am. Chem. Soc.*, 2016, **138**, 9401–9404.
126 Z. Wang, J. Cheng, X. Zhang, W. Yang, J.-Y. Park, H.-T. Kim and L.-H. Xu, *ACS Sustainable Chem. Eng.*, 2020, **8**, 15179–15188.
127 C. Zheng, L. Xiao, R. Qu, S. Liu, Q. Xin, P. Ji, H. Song, W. Wu and X. Gao, *Chem. Eng. J.*, 2019, **361**, 874–884.
128 B. Heidel and B. Klein, *Int. J. Coal Geol.*, 2017, **170**, 28–34.
129 R. Domínguez-González, I. Rojas-León, E. Martínez-Ahumada, D. Martínez-Otero, H. A. Lara-García, J. Balmaseda-Era, I. A. Ibarra, E. G. Percástegui and V. Jancik, *J. Mater. Chem. A*, 2019, **7**, 26812–26817.
130 X.-Z. Luo, X.-J. Jia, J.-H. Deng, J.-L. Zhong, H.-J. Liu, K.-J. Wang and D.-C. Zhong, *J. Am. Chem. Soc.*, 2013, **135**, 11684–11687.
131 Y. Wang, J. Yin, D. Liu, C. Gao, Z. Kang, R. Wang, D. Sun and J. Jiang, *J. Mater. Chem. A*, 2021, **9**, 2683–2688.
132 E. Gomez, M. Gutiérrez, B. Cohen, I. Hisaki and A. Douhal, *J. Mater. Chem. C*, 2018, **6**, 6929–6939.
133 T. Cheng, J. Hu, C. Zhou, Y. Wang and M. Zhang, *Sci. China: Chem.*, 2016, **59**, 929–947.
134 Z. Hu, B. J. Deibert and J. Li, *Chem. Soc. Rev.*, 2014, **43**, 5815–5840.
135 Y. Shu, Q. Ye, T. Dai, Q. Xu and X. Hu, *ACS Sens.*, 2021, **6**, 641–658.
136 X. Liu, D. Huang, C. Lai, G. Zeng, L. Qin, H. Wang, H. Yi, B. Li, S. Liu, M. Zhang, R. Deng, Y. Fu, L. Li, W. Xue and S. Chen, *Chem. Soc. Rev.*, 2019, **48**, 5266–5302.
137 I. Hisaki, N. Ikenaka, S. Tsuzuki and N. Tohnai, *Mater. Chem. Front.*, 2018, **2**, 338–346.
138 I. Hisaki, S. Nakagawa, N. Tohnai and M. Miyata, *Angew. Chem., Int. Ed.*, 2015, **54**, 3008–3012.
139 I. Hisaki, N. Ikenaka, N. Tohnai and M. Miyata, *Chem. Commun.*, 2016, **52**, 300–303.
140 I. Hisaki, H. Toda, H. Sato, N. Tohnai and H. Sakurai, *Angew. Chem., Int. Ed.*, 2017, **56**, 15294–15298.
141 I. Hisaki, Y. Suzuki, E. Gomez, Q. Ji, N. Tohnai, T. Nakamura and A. Douhal, *J. Am. Chem. Soc.*, 2019, **141**, 2111–2121.
142 E. Gomez, Y. Suzuki, I. Hisaki, M. Moreno and A. Douhal, *J. Mater. Chem. C*, 2019, **7**, 10818–10832.
143 I. Hisaki, Q. Ji, K. Takahashi, N. Tohnai and T. Nakamura, *Cryst. Growth Des.*, 2020, **20**, 3190–3198.
144 Z. Ke, K. Chen, Z. Li, J. Huang, Z. Yao, W. Dai, X. Wang, C. Liu, S. Xiang and Z. Zhang, *Chin. Chem. Lett.*, 2021, **32**, 3109–3112.
145 Y. Yang, L. Chen, F. Jiang, M. Yu, X. Wan, B. Zhang and M. Hong, *J. Mater. Chem. C*, 2017, **5**, 1981–1989.
146 S.-N. Zhao, L.-J. Li, X.-Z. Song, M. Zhu, Z.-M. Hao, X. Meng, L.-L. Wu, J. Feng, S.-Y. Song, C. Wang and H.-J. Zhang, *Adv. Funct. Mater.*, 2015, **25**, 1463–1469.
147 T. Feng, Y. Ye, X. Liu, H. Cui, Z. Li, Y. Zhang, B. Liang, H. Li and B. Chen, *Angew. Chem., Int. Ed.*, 2020, **59**, 21752–21757.
148 H. Li, W. Han, R. Lv, A. Zhai, X.-L. Li, W. Gu and X. Liu, *Anal. Chem.*, 2019, **91**, 2148–2154.
149 J.-f. Feng, T.-f. Liu, J. Shi, S.-y. Gao and R. Cao, *ACS Appl. Mater. Interfaces*, 2018, **10**, 20854–20861.
150 L. Wu, Y. Sun, K. Sugimoto, Z. Luo, Y. Ishigaki, K. Pu, T. Suzuki, H.-Y. Chen and D. Ye, *J. Am. Chem. Soc.*, 2018, **140**, 16340–16352.
151 H. A. Al-Attar and A. P. Monkman, *Adv. Funct. Mater.*, 2012, **22**, 3824–3832.
152 G. Cui, X. Yang, Y. Zhang, Y. Fan, P. Chen, H. Cui, Y. Liu, X. Shi, Q. Shang and B. Tang, *Angew. Chem., Int. Ed.*, 2019, **58**, 1340–1344.
153 Y. Yang, Q. Zhao, W. Feng and F. Li, *Chem. Rev.*, 2013, **113**, 192–270.
154 L. Bian, H. Shi, X. Wang, K. Ling, H. Ma, M. Li, Z. Cheng, C. Ma, S. Cai, Q. Wu, N. Gan, X. Xu, Z. An and W. Huang, *J. Am. Chem. Soc.*, 2018, **140**, 10734–10739.
155 H. Dong, Y. Wei, W. Zhang, C. Wei, C. Zhang, J. Yao and Y. S. Zhao, *J. Am. Chem. Soc.*, 2016, **138**, 1118–1121.
156 J. Xing, X. F. Liu, Q. Zhang, S. T. Ha, Y. W. Yuan, C. Shen, T. C. Sum and Q. Xiong, *Nano Lett.*, 2015, **15**, 4571–4577.
157 W. Zhang, J. Yao and Y. S. Zhao, *Acc. Chem. Res.*, 2016, **49**, 1691–1700.
158 X. Liu, Q. Zhang, J. N. Yip, Q. Xiong and T. C. Sum, *Nano Lett.*, 2013, **13**, 5336–5343.
159 J. Zhao, Y. Yan, Z. Gao, Y. Du, H. Dong, J. Yao and Y. S. Zhao, *Nat. Commun.*, 2019, **10**, 870.
160 Z. Bai, X. Yan, Z. Kang, Y. Hu, X. Zhang and Y. Zhang, *Nano Energy*, 2015, **14**, 392–400.
161 K. Na, K. M. Choi, O. M. Yaghi and G. A. Somorjai, *Nano Lett.*, 2014, **14**, 5979–5983.

162 S. Yan, X. Guan, H. Li, D. Li, M. Xue, Y. Yan, V. Valtchev, S. Qiu and Q. Fang, *J. Am. Chem. Soc.*, 2019, **141**, 2920–2924.
163 S. Qiao, B. Zhang, Q. Li, Z. Li, W. Wang, J. Zhao, X. Zhang and Y. Hu, *ChemSusChem*, 2019, **12**, 5032–5040.
164 W. Wang, Y. Zhang, L. Chen, H. Chen, S. Hu, Q. Li, H. Liu and S. Qiao, *Polym. Chem.*, 2021, **12**, 650–659.
165 B. Zhang, W. Wang, L. Liang, Z. Xu, X. Li and S. Qiao, *Coord. Chem. Rev.*, 2021, **436**, 213782.
166 Y. Zhao, J. Zhao, Q. Li, C. Gu, B. Zhang, C. Liu, Z. Li, S. Hu and S. Qiao, *Electrochim. Acta*, 2020, **331**, 135436.
167 Q. Guo, C. Zhou, Z. Ma and X. Yang, *Adv. Mater.*, 2019, **31**, 1901997.
168 B. Yu, L. Li, S. Liu, H. Wang, H. Liu, C. Lin, C. Liu, H. Wu, W. Zhou, X. Li, T. Wang, B. Chen and J. Jiang, *Angew. Chem., Int. Ed.*, 2021, **60**, 8983–8989.
169 X.-T. He, Y.-H. Luo, Z.-Y. Zheng, C. Wang, J.-Y. Wang, D.-L. Hong, L.-H. Zhai, L.-H. Guo and B.-W. Sun, *ACS Appl. Nano Mater.*, 2019, **2**, 7719–7727.
170 D. Yi, T. Bayer, C. P. S. Badenhorst, S. Wu, M. Doerr, M. Höhne and U. T. Bornscheuer, *Chem. Soc. Rev.*, 2021, **50**, 8003–8049.
171 S. Hudson, J. Cooney and E. Magner, *Angew. Chem., Int. Ed.*, 2008, **47**, 8582–8594.
172 W. Liang, H. Xu, F. Carraro, N. K. Maddigan, Q. Li, S. G. Bell, D. M. Huang, A. Tarzia, M. B. Solomon, H. Amenitsch, L. Vaccari, C. J. Sumby, P. Falcaro and C. J. Doonan, *J. Am. Chem. Soc.*, 2019, **141**, 2348–2355.
173 Q. Sun, C.-W. Fu, B. Aguila, J. Perman, S. Wang, H.-Y. Huang, F.-S. Xiao and S. Ma, *J. Am. Chem. Soc.*, 2018, **140**, 984–992.